

Chapter 11

Detector Simulation



J. Apostolakis

This chapter provides an overview of particle and radiation transport simulation, as it is used in the simulation of detectors in High Energy and Nuclear Physics (HENP) experiments and, briefly, in other application areas. The past decade has seen significant growth in the availability of large networked computing power and particle transport tools with increasing precision available to HENP experiments, and enabled the use of detailed simulation at an unprecedented scale.

After describing the uses of detector simulation and giving an overview of its components, we will examine selected cases and key uses of detector simulation in experiments and its impact.

11.1 Overview of Detector Simulation

11.1.1 Uses of Detector Simulation

Simulating the generation of particles in an initial collision, the interaction of these primaries and their daughter particles with the material of a detector and the response of the detector is a key element of recent experiments. Its importance has grown with each generation of experiments from LEP, B-factories, and the Tevatron, through to the current generation at the LHC, due to the increased precision requirements. It will be a significant element in planned experiments at super-B factories, the International Linear Collider (ILC), the Future Circular Collider (FCC), and also for numerous ongoing and smaller future experiments.

J. Apostolakis (✉)
CERN, Geneva, Switzerland
e-mail: john.apostolakis@cern.ch

© The Author(s) 2020
C. W. Fabjan, H. Schopper (eds.), *Particle Physics Reference Library*,
https://doi.org/10.1007/978-3-030-35318-6_11

Simulation serves many purposes at each point in the lifecycle of an experiment or a facility. Different types of simulation are used, typically with an increasing level of detail during a lifecycle. At first, fast simulation follows only the most energetic particles, typically the particles arising from the primary interaction, through simplified geometrical descriptions to obtain average values for energy deposition in the key volumes in which a signal is generated. Later, in more detailed simulation, the interactions create secondary particles, which in turn are tracked and create further descendant particles; interactions are treated with more detail and energy deposition includes fluctuations. This enables the estimation of many quantities including the measurement resolution of detectors, and correlations.

To prepare a proposal for an experiment, different versions of the setup are simulated. For each design a simplified version is constructed and simulated, typically using a tool such as SLIC [1] or DDG4 [2] which provide templates for detector components and hit generation. Putting this together with tailored digitization and reconstruction, many key characteristics of a design necessary for technical design report [3] can be evaluated.

The energy dispersion or resolution of calorimeters, the longitudinal and lateral leakage, corrections to momentum measurements, the backscattering of particles into trackers or other ‘upstream’ components can be estimated for different designs. Accurate simulation is a powerful quantitative tool for optimizing the performance, the size and cost of each sub-detector. In addition, its use extends to quantifying the tradeoffs between the performance of combinations of detectors, and finally for optimizing the global performance of a complex modern detector.

During the prototyping and calibration phase of a detector, simulation is utilized for test beam setups of single detectors or combinations to ensure that their performance is understood and can be accurately modeled. The accuracy expected in today’s high precision experiments requires agreement between simulation and test beam measurements at the level of 1% or better. This type of high-quality quantitative comparison is the basis for evaluating through simulation significant corrections to measurements in the experiment that cannot be obtained in a test beam or directly from in-situ data once the experiment starts operating.

The possibility for detailed modeling of the conversion of energy deposition into signal within a detector is a key strength of detector simulation. This requires detailed knowledge of many detector-specific effects. Simulation is an important tool also for the data analysis phase of an experiment. After its accuracy has been validated against single-particle benchmarks and test beams, an experiment’s simulation can be utilized to model tracks of different types, and even full signal and background events. Detailed quantitative aspects of simulated tracks are used in preparing methods for particle identification and measurement before the start of an experiment, and continue to be crucial in many methods that utilize data to calibrate complex quantities such as the jet energy scale. It can also be used in modeling the separation of signal from background contributions to measured data.

The impact of a performant detector simulation, whose predictions matched data, was demonstrated in the first years of the operation of the LHC experiments, during

which reconstruction and calibration in many channels were achieved within the first years of operation, a fraction of the time of previous hadron collider experiments [4].

A challenging aspect of the use of simulation in data analysis is the estimation of the systematic errors of the simulation. The accuracy of a simulation depends on the accuracy of the description of the detector's geometry and material composition, the knowledge of the beam or primary particles delivered and the intrinsic accuracy of the simulation tool(s) used. The detector simulation tools, in turn, are limited by several factors: the availability and known accuracy of measurements utilized to tune or validate the physics models, in particular of the cross-sections; the limitations of the physical models in reproducing the energy spectra and other properties of interactions; the approximations utilized to obtain adequate computational speed, to simulate the required number of events using the available computing resources.

There is an important tradeoff between the level of detail, both in the geometrical description of a setup and the choice of physics modeling options, and the computational cost of large-scale simulation. In the past 5 years the LHC experiments have been able to use detailed simulation to produce several billion events per year [5] providing unprecedented support of analysis in hadron collider physics. The increase in luminosity in the HL-LHC era will bring a need for much higher statistics of simulated events, whereas projected growth in computing power is forecast to be modest in comparison [6]. This is driving research to achieve substantial performance gains in full simulation in GeantV [7], and the expectation that faster approximate simulation will be relied upon once again for most analyses—leading to efforts to create new kinds of fast simulation which more accurately capture additional features of the full simulation, including fluctuations of key quantities.

11.2 Stages and Types of Simulation

- Event generators and detector simulation
- Scale from full detail to fast simulation
- Simulation of energy deposition or signal generation
- Assessment of radiation effects
- Key tools: Event generators, detector Monte Carlo, radiation transport
 - Detector Monte Carlo: GEANT, FLUKA, GEANT4
 - Radiation related MC: FLUKA, MARS, MCNP/MCNPX
 - Signal generation: Garfield

The simulation of the passage of particles through a detector and the response of the detector's sensitive elements typically proceeds in different stages. In the first stage an external event generator simulates the initial interaction and then decays short-lived particles; the results are the “primary” tracks. The second stage is detector simulation and involves the tracking of the primary particles through the structures of the detector, sampling interactions with their components, and creating

secondary particles. In the third stage the “hit” information is processed, to estimate the signals that result.

In detector simulation the secondary particles and their descendant particles are tracked in turn. Information about the passage of particles through the sensitive parts of the detector is recorded as ‘hit’ information. For tracking detectors usually the individual position, momentum and particle type or charge information of each track is recorded; in calorimeters, the energy deposition within a cell is kept as a sum over all tracks. A key characteristic of detector simulation is that tracks are treated independently. Each particle created is tracked in turn, until all have exited the setup, suffered a destructive interaction, or have been dropped as unimportant according to a user’s chosen criteria. The dropping can be triggered, for example, when the energy of a track falls below a threshold or arrives in a particular ‘unimportant’ region. Potential indirect interactions between particles are not treated as part of the detailed simulation. As such, the creation of space charge in a gaseous detector must be introduced in an experiment’s ‘user’ code or else treated separately.

11.2.1 Tools for Event Generation and Detector Simulation

The creation of the primary particles by the high-energy interaction is modeled using specialized event generators. The type of interaction, energy range and applicability of these generators differ significantly: whether they include hadron–nucleus and/or nucleus–nucleus interactions, or the type of physics beyond the standard model they provide. Typically event generators are independent programs: including the established PYTHIA [8] and FRITIOF [9], which use the Lund fragmentation model [10], and more recent ones such as HERWIG [11]/HERWIG++ [12]. Most provide users with tunable parameters and the ability to create sets of parameter values (‘tunes’) compatible with the most relevant reference data at the energies of interest.

Some Monte Carlo tools include high-energy event generators: e.g. DPMJET is available in FLUKA, and has been used to simulate ion–ion collisions at RHIC and the collisions of high-energy cosmic rays in the atmosphere.

Codes for the simulation of the detector must handle geometries of significant complexity and a large number of volumes and they must model the full set of hadronic, electromagnetic and weak interactions as accurately as required, potentially within constraints of CPU time. In the past 20 years different tools have been used for this purpose, including GEANT 3, FLUKA and GEANT4. Other multi-particle codes for particular applications including the MARS [13, 14] code, and the SHIELD code which focus on ion–ion interactions. Different codes share some physics models; for example PHITS and MARS share several models with MCNPX, an extension of the neutron-gamma gold-standard code MCNP.

GEANT version 3 [15] was utilized by LEP experiments (ALEPH, L3), the TeVatron experiments at Fermilab, numerous other experiments and also by the ALICE experiment at LHC as its main simulation engine. It includes detailed descriptions of electromagnetic interactions down to 10 keV. For hadronic physics it

relies on external packages: GHEISHA [16], GCALOR [17], which uses CALOR89 [18], and GFLUKA, which interfaces to the 1993 version of FLUKA [19].

FLUKA [20], after a major overhaul in the 1990s, offers microscopic models for 60 elementary particles, all types of ions at energies from 1 keV to 10,000 TeV/A. It has been used for detector simulation by the Opera and ALICE experiments, in radiation assessment, accelerator collimation and target tuning, and many applications beyond HEP. A key emphasis and strength have been its single, consistent, core hadronic model, PEANUT, with a Dual Parton Model (DPM) based high energy cascade above 5 GeV, a generalized intranuclear cascade and suite of models for the excited nucleus. For nucleus–nucleus interactions above 5 GeV, it utilizes interfaces to DPMJET-III [21] event generator for interactions. There is an option for the detailed treatment of neutrons down to thermal energies, which uses the multi-group approach involving energy bins, and weighted averages of cross sections and interaction production. Physics processes for electromagnetic interactions and lepto-nuclear interactions are included. FLUKA focuses on a single set of physics processes, which are curated and validated extensively by its authors. A small set of optional variations of physics processes are provided, e.g. for the simulation of low-energy neutrons. The majority of uses in HEP lie outside detector simulation. Examples include the estimation of radiation backgrounds in experimental areas, whether in accelerator facilities or underground halls, and the modeling of beam interactions with collimators in accelerators. Extensive studies of the LHC radiation environment have been carried out using it over the past decade, and a FLUKA model of the full LHC collider is the production simulation for radiation studies.

GEANT4 [13] is the basis of the simulations of BaBar, ATLAS, CMS, LHCb and a large number of smaller experiments. Its standard configuration provides electromagnetic interactions for charged particles and gammas down to 1 keV, hadronic processes for nucleons, mesons and ions, models of electro-nuclear, lepto-nuclear interactions, radioactive decay of nuclei and optical processes for photons at visible and near-visible energies. A variety of hadronic processes has been used to span all projectiles at energies up to 1 TeV, with recent extension to 100 TeV for Future Circular Collider (FCC) applications [22]. An option for neutron interactions from 20 MeV down to thermal energies is available using cross-sections for individual elements and isotopes (a technique called ‘point-wise’). GEANT4 takes a toolkit approach, enabling and requiring its users to choose the parts required for their application area, including the configuration of physics models. Recommendations of physics model configurations are provided for several established type of application and for a number of HEP and external application domains; validations for several HEP applications have been undertaken in collaboration with experiments. For other application domains users are invited to undertake the appropriate validation, potentially using their specific data, and interacting with GEANT4 experts.

A few other codes provide extensive modeling of multiple particle types, including the PHITS [23] code and MCNP family. The most recent MCNP version 6 [24, 25] was created from the merger of MCNP5, which focused more on traditional neutron-gamma applications including simulation of nuclear facilities

and reactors and the all-particle offshoot MCNPX. Its models will be contrasted with the capabilities of FLUKA and GEANT4, but it has not seen use in HEP detectors, due to lack of electron/gamma models above 1 GeV, restrictive licensing and export control.

In order to compare with measurements, the response of detectors to the energy deposited by an event's tracks must be estimated. One tool used for the detailed estimation of the energy deposition in a gas detector is Garfield [26]. It generates low-energy gammas and electrons, down to eV energy using HEED [27], uses the electric field calculated externally, and transports electrons and ions under the combined influence of its electromagnetic field and diffusion. The recent Garfield++ rewrite [28] and extension extended its capabilities, added refined electron transport and physics models for semiconductors, and enabled interfacing with GEANT4 [29]. Its computational cost is 2–3 orders of magnitude larger, so it is utilized sparingly: for studies and to generate an accurate parameterization of a detector's response [30] for use in large scale simulations.

11.2.2 Level of Simulation and Computation Time

The modeling of every physical interaction, from the initial particle's energy down to the interaction of eV scale photons and electrons—or even the interactions of neutrons down to thermal energies—is possible. The computing cost of such simulation is prohibitive for most practical applications, and simplifications are required. Yet in some cases it is necessary to simulate down to very low energies, for example in order to estimate the activation of materials by neutrons.

In complex detectors, such as in an LHC detector, the full simulation of each event takes between 0.1 and a few minutes on modern computers, depending on the type of event (minimum bias or t/t-bar) and the region simulated (rapidity coverage). This limits the number of events that can be simulated.

In some applications the simulation effort can be reduced for many events: by simulating first the particles that are involved in the trigger. Otherwise, one may seek to limit the number of secondary particles generated or the total track length simulated, or to simplify the treatment of the most frequent interactions.

Another alternative is fast simulation. This involves selecting only a fraction of tracks for simulation, and approximating the detector and key physics interactions in order to reduce the computation time per event by one, two or more orders of magnitude. Fast simulation is a powerful tool for modern experiments, as it allows speedy turnaround to address changing conditions or assumptions, and to explore different model parameters at an affordable computing cost. It can be calibrated using full simulation, data or both. However it is not capable to estimate resolutions and correlations, and it can be harder to obtain systematic errors.

Recently ATLAS has created a hybrid simulation mode by selecting for detailed simulation the conical regions of the detector around the most energetic primary particles, and using fast simulation models for the remainder [31].

11.2.3 Radiation Effects and Background Studies

The background in a modern detector can be due to many factors, including remnants of past events, accelerator generated backgrounds, and the backscattering of particles by the detector's surroundings. These can require simulation, in order to determine their level and characteristics. Also in many cases effects of the experiment on its surroundings or its constituents such as activation must be estimated. Simulation is an essential component.

Tools that are utilized for these tasks include FLUKA and the MARS code [32]. In addition to inclusive physics models, where the whole interaction is simulated, MARS contains exclusive models, where the leading particles and a sample of other secondaries is produced by an interaction.

Biasing is a technique in which some 'unlikely' trajectories are enhanced by a large numerical factor and assigned a weight inverse to this factor, in order to rapidly estimate their effect. It is an essential component of background applications. In many cases a result cannot be obtained without it; in others it improves greatly the accuracy of the result. Good statistical accuracy can be achieved within a fraction of the computation time required for an unbiased, so-called 'analogue', calculation for means and similar observables. Correlations, widths and other second order observables can be obtained only in some cases and by recording key additional information during simulation.

MARS has been used for accelerator and background calculations for many facilities [14] and experiments [33]. FLUKA also has seen wide application in this domain.

11.3 Components of Detector Simulation

- Geometry description and navigation
- External fields
- Electromagnetic physics models
- Hadronic physics models
- Low-energy neutron interactions
- Accuracy of simulation
- Fast simulation
- Signal generation
- Biasing, production thresholds

A complete tool for simulating particle interactions and detector response must include the description of a detector's geometry and material, the input or selection of primary particles, the modeling of all relevant physical interactions and the extraction of information such as the energy deposition and particle passage (hits).

Most tools also account for the effects of external electromagnetic fields on charged particles, provide visualisation of the geometry and simulated events. They provide for tallies, output of key physical quantities calculated during the simulation, such as totals of energy deposition, dose, particle flux and fluence. They also provide the opportunity for the user's code to filter and record track quantities at each step.

The geometry module provides the ability to describe the material composition and the geometry of the setup in terms of volumes. The tool must be able to navigate inside this volume description, identify the volume in which a point is located and calculate the distance to the next boundary in a given direction. The capabilities of the geometry modeler determine the type of volumes and their relative placement: whether volumes are generated directly as finite shapes, or whether they are the result of the intersection of surfaces; whether all volumes must be placed within a single 'world' volume, or a hierarchy of volumes can be created. In order to simulate a large, complex detector with hundreds of thousands to millions of volumes, the geometry modeler needs to support hierarchical geometry definitions.

To ensure good performance the key geometry operations must be computationally efficient; in particular, the computation of the distance to intersecting a boundary is critical. Optimisation methods which rely on data precomputed at initialization inspired by ray-tracing are used to greatly reduce computation time wherever many candidate sub-volumes exist.

Some experiments have chosen to use a geometry modeler external to the simulation tool. They use the same geometry description and modeler inside a Virtual Monte Carlo framework [34]. This interfaces to different simulation tools for modeling interactions: GEANT, FLUKA and GEANT4; they are labeled 'physics engines' and can be selected at runtime.

11.3.1 External Fields

The effects of external electromagnetic fields on the trajectory and energy of a charged particle track are modeled utilizing the Lorentz equation. The equations of motion for the position, the momentum and optionally the polarisation of the particle are integrated to obtain the position and state of a particle after a distance s . In special cases, such as a constant magnetic field, an analytical solution can be used. In the general case, numerical integration is used, typically with a Runge-Kutta method.

After integration the idealized curved path of a particle track in a magnetic field is propagated through the geometry of a detector. The curved trajectory is split into linear chord segments, which are used to navigate in the model geometry. The intersection of a chord segment is progressively refined to identify the location where the curved path crosses a geometry boundary.

11.3.2 Introduction to the Transport Monte Carlo Method

At each step of a simulation, the Monte Carlo method for particle transport needs:

- the cross sections in the current material of each physical interaction;
- an algorithm to select which interaction occurs next;
- a method to apply the effects of each interaction: to generate new particles, and change the state of the potential surviving projectile.

The Monte Carlo method [35], general techniques [36] and its application to particle transport for charged and neutral particle transport [37] are well described in the literature. We touch on a few of the essential features.

A key ingredient is a source of ‘pseudorandom’ numbers, distributed uniformly in an interval, usually [0,1). These are obtained from pseudorandom number generators [38] and must come with guarantees of non-correlation, such as those provided by the generators based on ergodic theory, MIXMAX [39, 40] and RANLUX [41, 42], or at least have survived a barrage of empirical tests [43] to suggest there are no correlations which affect the Monte Carlo estimates.

For a general particle the total interaction cross-section (summed over all interactions)

$$\sigma_{\text{total}} = \sum_i \sigma_i$$

is used to sample the step length s , using a random number r from the interval (0,1):

$$s = -(1/\mu) \ln r$$

where the absorption coefficient μ is proportional to the cross-section σ_{total} and density ρ . Thereafter, the type of interaction that will occur at this step is chosen. The probability for one particular type of interaction to occur (in one step) is proportional to its cross section.

In the ideal case, all interactions would be sampled this way. However, in practice a different approach is needed, as the cross section diverges for the emission of soft photons and delta rays. A systematic treatment proposed by Berger [44], separates collisions that alter the state of the particle below a chosen threshold, typically for the momentum transfer. These are not sampled individually; only their collective effect is sampled. The collisions above the threshold are simulated individually.

In this approach, the part of the cross section corresponding to an interaction below this threshold is labeled the continuous part, and it does not contribute to limiting the step. Its effect is applied separately as an integral over the length of the step, to the state of a track.

The discrete part of an interaction contributes its cross-section to limiting the step

$$\sigma = \sigma_{\text{discrete}} + \sigma_{\text{continuous}}$$

Its cross section represents all interactions resulting in secondary particles with energy E above the threshold energy E_0 :

$$\sigma_{discrete} = \int_{E_0}^{\infty} \frac{d\sigma}{dE} dE$$

This treatment is required for the Bremsstrahlung process and delta-ray production, due to the large number of secondaries produced with low energy.

11.3.3 Electromagnetic Interactions and Their Modeling

The modeling of physical processes can be separated into models of electromagnetic (EM) interactions, models of hadronic interactions (involving the strong nuclear force) and the decay of unstable particles mediated by the weak force. The Monte Carlo simulation of EM interactions of charged particles with atoms has been well established in HEP applications since the advent of EGS4 in the 1980s. EGS4 was able to produce and track photons, electrons and positrons down to 10 keV.

At typical HEP energies of 1–100 GeV, the number of particles of the electromagnetic shower is large. The full simulation of all resulting particles is costly in computational resources, and a selection of particles is undertaken to represent the shower. Typically, particles are tracked until they reach a certain energy threshold, the tracking cut, and discarded. In addition, secondary particles are emitted only if their energy is above a chosen energy, called the production threshold. For specific applications the high density of energy deposition near the endpoint of a track (Bragg peak) is relevant, and can be simulated.

Electromagnetic interactions of gamma-ray photons include Compton scattering, the photoelectric effect and, gamma conversion, the production of electron–positron pairs. Cross sections for each process are calculated directly from theoretical or empirical formulae, or parameterized. For example the Klein-Nishina formula is used for the cross section of Compton scattering. To improve execution speed the value of the cross sections are pre-calculated at several energies; the value at any other energy is obtained by interpolation.

The method used to model multiple scattering, in particular near boundaries, is a key feature of a simulation tool. Obtaining accurate results using less computing power, and obtaining results that are stable when varying parameters (such as the production threshold or tracking cut) are significant algorithmic challenges.

The EGS approach for the simulation of photons and electrons and its implementation were pioneered by Nagel. It was improved and shared within the HEP community as the EGS3 [45] and EGS4 [46] code systems. From these other HEP codes for EM interactions are descended, or inspired.

The underlying assumptions in Monte Carlo simulation of radiation transport are the same amongst these and modern codes: materials are assumed to be amorphous,

and beam particles do not interact. The methods for modelling transport of photons and electrons used in Monte Carlo codes are based on sampling of differential cross sections obtained from approximate theoretical calculations. A recent review offered a comprehensive description of the principles and approximations [47] for models of electron and photons up to 1 GeV, documenting widely used models and those of the precise modern electron–photon code Penelope [48].

11.3.4 Interactions of Photons

Photon interactions are ‘discrete’ interactions, that occur at a point and can be modeled this way. This makes them much simpler than modeling the interactions of charged particles. Interactions considered including photoelectric, Compton incoherent scattering, electron–positron pair production and potentially Rayleigh coherent scattering.

The cross section for each interaction is sampled from measured or theoretical distributions. In some cases a simplified form is used, to reduce the cost of computation with a simplified description of the energy and Z dependence. Else, the values for each material at particular values can be pre-computed and stored in tables for interpolation.

Once the type of interaction is chosen, its products are sampled from the appropriate distributions. Pseudorandom numbers are used to sample the energy, angles and momenta from the differential distributions [37]. The original particle’s state, if it survives, is altered to preserve energy and momentum.

The interaction of energetic photons with nuclei is discussed in the hadronic section below. Often specialized tools are used to simulate optical photons and their collection. It is possible, though, to generate optical photons and model reflection, refraction and absorption on different types of surfaces. GEANT4 is able to do this.

11.3.5 Interactions of Charged Particles

The simulation of the electromagnetic (EM) interactions of charged particles is complicated by the large cross section for elastic interactions and of ionization, which produces low-energy electrons (delta electrons).

In a few cases it is useful to simulate every single interaction of a charged particle in a medium, including its elastic collisions with nuclei, the ionization of atoms and creation of delta electrons, and the ‘hard’ interactions, which create photons or electron–positron pairs.

All production simulation tools estimate the cumulative effect of the elastic scattering off nuclei. It is modeled in several different ways. Many utilize the multiple-scattering approach pioneered by Goudsmit and Sanderson [49] as their basis. One simple way to sample angular deviation over a short step is Moliere’s

theory [50], which is used in GEANT 3, but is limited to small angles. The approach of GEANT4 borrows from Lewis' description [51].

Key effects of multiple scattering are angular deflections and straggling. The latter's most important effect is the shortening of the distance travelled in the direction of the initial momentum. This must be modeled in order to obtain correct energy loss for the passage through material, as is done in GEANT 3. The second effect of straggling, the displacement in the lateral directions is correlated with angular deflection. Similarly to EGS4, FLUKA and GEANT4 also sample this displacement, each using different algorithms. This enables longer steps while maintaining accuracy. The best algorithms allow longer steps, or more accurate modeling of the correlations between the affected changes in the state of the particle.

The algorithm for multiple scattering has a significant effect on the results obtained in many detectors and setups. Examples include the partition of energy in sampling calorimeters, the correlation between the deflection of muons and their positions after substantial material. In particular, many quantities are very sensitive to the details of its formulation and implementation. These include the fraction of low-energy electrons ($T \ll 1$ MeV) scattering backwards at the interface between low and high Z materials and the correlation between the direction of a particle exiting a detector (e.g. muon) and its position.

In addition to the sampling of the final state, high accuracy for electron transport necessitates careful treatment of multiple scattering of low-energy electrons at boundary crossing [52]. New algorithms have been developed for exact electron transport without special treatment for boundary crossing [53, 54]. These algorithms have been implemented in electron-photon Monte Carlo codes: PENELOPE [55], EGSnrc [56] and EGS5 [57]. A comparison [58] in 2007 benchmarked the algorithms in several of these codes and in GEANT4, using data from custom setups with thin slabs. PENELOPE and EGSnrc demonstrated the best performance, while GEANT4 obtained good results only with specific settings.

The new GEANT4 GS model [59], available since GEANT4 release 10.3, implements Kawrakow's approach to provide angular deflections for any size step without free parameters and offers the option for accurate boundary crossing. It achieves the best agreement, amongst GEANT4 models, with a wide range of benchmark data including backscattering data.

Models for specialized processes, such as transition radiation, exist in some tools including GEANT4 [60].

11.3.6 Hadronic Interactions and Their Modeling

In contrast to the simulation of EM physics processes, the simulation of hadronic physics processes from first principles is not possible, except partially at the high energy limit. At all energies, the cross-sections and the models used are based, directly or indirectly, on measured data of hadron-nucleon and hadron-nucleus interactions, and on phenomenology.

The most common particles produced by hadronic interactions are nucleons, pions and kaons. The diversity of particles and interactions make modeling a great challenge. Specialised codes including HETC [61], GHEISHA, CALOR [18], FLUKA, and SHIELD [62] were developed for HEP and other application areas in the 1970s and 1980s. Few models and codes from other application domains have been available which cover a substantial part of the energy range (above the 1–2 GeV used in spallation applications) and the full set of particles needed for HEP. One exception is the MCNPX tool, an extension of the MCNP code for neutron/gamma radiation transport and reactor simulation. MCNPX hadronic models are shared with MARS.

Interactions are divided into elastic and inelastic, which produce new particles in the final state. The smaller cross-sections for inelastic interactions of hadrons with nucleons compared to EM interactions, and the growing multiplicity and variety of particles emitted in interactions above a few GeV, result in significantly different structure for hadronic showers.

The modeling approach depends on several factors: the availability of detailed experimental measurements; the complexity of final states of reactions for a particular combination of incident particle, energy and target; and the availability and suitability of theoretical or phenomenological descriptions. In many application domains there is a requirement for conservation of energy, momentum and quantum number in each interaction, and for the coincidence or correlation between the products of an interaction; in selected cases conservation of energy only as an average over different interactions may suffice. A small number of interaction models, including GHEISHA, and most low-energy neutron interactions sampling methods treat particle interactions only in the average, and do not conserve energy and momentum.

For many applications full energy conservation of individual interactions and the treatment of the correlations of particle tracks is required in order to obtain reliable results. For example, the estimation of the energy resolution of hadronic calorimeters is strongly affected by these factors.

In many cases a phenomenological model is supplemented by fits of model parameters with available data. In a few cases (evaluated) data libraries are used directly—typically for low-energy neutron transport. Another approach is to use parameterizations, either directly of data or indirectly for the parameters of simplified models, as in GHEISHA.

11.3.7 Models of Interactions at Low Energies

At the lowest energies, the largest hadronic cross section belongs to the elastic interaction, which is a coherent interaction of a hadron projectile with the full nucleus. Hadronic cross sections, including those for elastic scattering, are typically parameterized from data.

Inelastic interactions, which excite the nucleus, typically become relevant at energies of order MeV. They are modeled with a statistical approach for energies up to about 100 MeV. The original Weisskopf evaporation model [63] describes the emission of protons and neutrons from nuclei in thermodynamic equilibrium. It is supplemented by several additional de-excitation channels, which compete to occur. These include the multi-fragmentation model for highly excited nuclei [64], Fermi breakup of light nuclei, fission of heavy nuclei and photon evaporation.

In an alternative approach, following the Generalised Evaporation Model (GEM) of Furihata [65], nuclei with up to 28 nucleons are evaporated directly. This improves greatly the description of the emission of light and medium fragments, with an extra computational cost. GEM is an option in MCPNX, in GEANT4 and a similar approach is used in FLUKA. Fragments heavier than ^4He , though emitted infrequently, are important for specific applications, such as the response of silicon devices and damage to them; using the GEM approach is recommended for these.

At energies up to about 300 MeV a simple algorithm can be used to count the number of excited nucleons and holes of missing nucleons in the Cascade Exciton Model (CEM) model [66]. Such models are called pre-compound (or pre-equilibrium) models. A pre-compound model of this type is implemented in GEANT4. And CEM.03 [67], which is included in MARS, MCNPX and MCNP 6, is an improved CEM descendant.

These models are also used to calculate the de-excitation of nuclei after interactions at the higher energies, important in many applications. For example, they determine the energy that is lost to nuclear breakup, and the partitioning of energy between the low-energy protons, neutrons and gammas that are produced. These processes produce the majority of neutrons, whatever the initial interaction, and as a result affect substantially the escaping energy, lateral shower profiles and compensation of calorimeters—amongst other observables.

11.3.8 Cascade Models of Hadron–Nucleus Interactions at Intermediate Energy

At energies above about 100 MeV an intranuclear cascade model is used for nucleon and pion projectiles. In a cascade the interaction is modeled as a succession of independent collisions of the projectile (and secondaries) with individual nucleons inside the target nucleus [68].

In a cascade, the nucleus is described in two ways. It can be an ensemble of nucleons positioned at random locations, sampled from a model of nuclear density—as used Quantum Molecular Dynamics (QMD) models such as UrQMD [69], in the GEANT4 Binary cascade model [70] and in the Liege cascade INCL. Else, the nucleus can be composed of a number of shells of constant density, as in the original cascade of Bertini, in FLUKA, and in INUCL and its descendant, the

GEANT4 Bertini-type cascade [71]. A correction factor is used for the depletion of nuclear shells by earlier interactions in both FLUKA and GEANT4 Bertini.

It uses ‘free-space’ cross-sections derived from hadron–proton measurements, or, in some cases cross-sections modified for the presence of the nuclear medium [72]. FLUKA accounts for nuclear medium effect on the Δ resonance properties in the treatment of pion interactions [20].

Hadrons may move in curved trajectories according to a chosen nuclear potential, as in GEANT4 Binary and FLUKA, or in straight lines (GEANT4 Bertini). In both cases, the potential is used to update the momentum of all hadrons before interactions. Interaction products can use models or be sampled from data, must observe the Pauli exclusion principle, and are subject to a hard-core nucleon repulsion. Particles arriving at the nuclear boundary with enough energy are ejected, while others are reflected and continue to interact. The difference of the total energy of the remaining nucleons and the ground state energy that corresponds to them is the excitation energy.

After either a fixed time or once the excitation energy has dipped below a threshold, the remaining nucleons are handed to a pre-equilibrium or de-excitation module. A pre-equilibrium model, such as the Precompound model, can eject higher energy nucleons and is used with the GEANT4 Binary cascade. A similar model is used in FLUKA. The subsequent de-excitation module combines evaporation, Fermi-breakup for light nuclei, fission for heavy nuclei and other competitive channels.

A common de-excitation module is shared by all models in FLUKA. A custom simpler de-excitation module is used in GEANT4 Bertini; recent extensions enabled it to use the default “Preco” Pre Compound and de-excitation module, used after Binary cascade and the higher energy string models (QGS and FTF). In MCNPX, MARS and MCNP a common module is used with different parameters by the CEM cascade and the higher energy LAQGSM [67] model.

Most cascade models are expected to work up to 1.5–3 GeV, yet they can provide good results from 30 MeV up to 3–5 GeV. At higher energies their assumptions break down, because quark degrees of freedom become important. Including additional reactions with larger multiplicities of products, and effects such as formation time (a simplified treatment of quantum-mechanical effects as a time interval before secondary hadrons can interact) allows a cascade model to have a higher energy limit. This is the case for the GINC/PEANUT cascade in FLUKA and the GEANT4 Bertini cascade.

Early versions of GEANT4 until 9.6 also included the CHIPS model [73] applicable for intermediate energies. It described a nucleus in terms of nucleon clusters, and interactions as exchanges of quarks and was part of physics lists used in LHC Run 1.

The GEANT4 Bertini cascade underwent a substantial rewrite and upgrade [74]. As a result, all long-lived hadrons can be projectiles (adding K, Λ , Σ , Ξ and Ω). It also implements gamma- and lepto-nuclear reactions. Its energy range was extended up to 15–20 GeV, with the addition of final states with higher multiplicities, up to nine for proton–proton. Total and partial cross sections and final states were obtained from the CERN-HERA data compilations, and completed using symmetries and

general principles for unmeasured reactions and energies. The number of nuclear shells varies from one for the light, three for medium, and a maximum six for the heaviest elements.

As its main use is the simulation of LHC experiment detectors, a number of modeling and implementation choices were made to optimize computation speed. These include linear interpolation for the sampling of partial cross sections and large 10-degree bins in angular distributions—justified by the smoothing effect of additional interactions.

The newest cascade model in GEANT4, the INCL Liege cascade, is the one under the most active development. This event generator, under development since the 1990s [75], was developed to reproduce spallation data for reactions at 100 MeV–1.5 GeV using a parameter-free model. It interfaced with the ABLA code for deexcitation. Its original Fortran version up to version 4.6 [76] has interfaced to MCNPX and MCNP6. Recent development focused on the re-engineered INCL++ [77], which reproduced the performance of 4.6 and was extended to handle light ion projectiles (up to carbon16) and to higher energies, up to 15 GeV producing multiple pions.

Large suites of benchmark data are used to tune and verify the modeling of each cascade, covering neutron, proton and pion production at energies from 60 MeV to 3 GeV. Spallation data from inverse kinematic reactions on hydrogen targets at GSI with a range of projectiles from ^{56}Fe [78] to ^{238}U [79] at 1 GeV/nucleon provide different challenges for modeling and complement these data.

Comparisons of hadronic and in particular cascade models have been undertaken periodically under the auspices of the IAEA [80]. These benchmarks use a large set of thin target data to probe the accuracy and predictive capabilities of each model. INCL was found to be one of the competitive models. Similar test suites are utilized as a part of internal benchmarks and for tuning of models.

The details of the intranuclear cascade and the pre-equilibrium model determine all the emission of higher energy particles, but the details of the coupling and the quality of the de-excitation module are also critical to the performance of many applications from activation to calorimeter simulation. Good modelling of the resulting nuclei is required to ensure that the energy lost to nuclear breakup, a key component of non-compensation in hadronic calorimeters, is accurate. Recent results from RD52 [81] were interpreted as deficiencies in the modelling of nuclear breakup in GEANT4 version 9.4, showing that there is room for further improvement in this energy range.

11.3.9 High-Energy ‘String’ Models

Models for interactions at high energies (above 5–10 GeV) simulate quark-level interactions and rely on phenomenological descriptions of soft QCD interactions to generate low-energy hadrons from the remnants of the high-energy collisions. They are applicable to all hadron projectiles. Three variants are available: the Dual Parton

model [82] is implemented in DPMJET [21] and used in FLUKA. The Quark Gluon String (QGS) Model [83] in different variants is used in MARS/MCNPX, GEANT4 and in the QGSJET event generator [84]. A third model, the Fritiof model, is used and extended in the FTF model in GEANT4.

Hadrons are produced in the initial collisions and the decay of QCD strings, tubes composed of compressed gluonic fields [10] generated by the separation of colored quarks. Models implement a Lund-like string. The proto-hadrons generated by string decay, once past their formation time, together with outgoing nucleons, and the remaining cluster of nucleons are handed to a cascade for additional scattering in the nucleus (e.g. in FLUKA and in GEANT4 QGS_BIC and FTF_BIC physics lists using the Binary cascade), or passed directly to a pre-compound module (in the GEANT4 QGSP_BERT and FTFP_BERT physics list).

Developments over the last 10–15 years include a high-energy extension of the PEANUT cascade in FLUKA to undertake reactions handled previously by DPMJET; the connection of the Binary cascade in GEANT4 with the QGS model (as QGS_BIC) to re-scatter the slow products of high-energy model. More recent developments include the extensive improvement of the Fritiof-based FTF model in GEANT4 to model light anti-nucleus interactions at low energies and at rest [85], and to include an internal Regeon cascade, and changes in the production ratio of different types of diquarks [86].

11.3.10 Treatment of Low-Energy Neutron Interactions

Amongst particles created by hadronic interactions, neutrons survive a longer time and are among those which travel the furthest. Also, they are amongst the most numerous. This makes their treatment important for many applications and correspondingly expensive computationally. Most neutrons are emitted in the de-excitation phase of a reaction and have energies of order MeV.

Neutrons produced in high-energy interactions (above 20 MeV) also lose energy in elastic and inelastic interactions (which release protons, alpha particles or light ions—or create gamma rays) before being captured by nuclei. Only part of this process occurs on fast timescales and others are much slower (μs –ms). By tracking time, it is possible to emulate the time dependence of the signal. This also allows the simulation tool to use a time threshold, and abandon neutron tracks after this time, in order to save computation time.

Neutrons' contribution to the visible energy measured in a detector comes via the transfer of energy to charged particles and from capture and other reactions with nuclei that generate gammas. Elastic scattering is particularly important in organic scintillators, where interactions with hydrogen transfer significant parts of energy and momentum to the recoil proton.

In some cases, are treatment of neutron interactions at a greater level of detail is required, potentially down to thermal energies. In HEP it is needed in special cases, such as the study of activation of materials for radiation safety purposes.

The detailed treatment of energy deposition in scintillators may also require a more detailed treatment of neutrons than provided by the simpler interaction models.

Simulating neutrons below 20 MeV relies on measurements of cross-sections for key processes, which have been assembled into established data libraries. Libraries, such as JEFF [87], ENDF/B VII [88], ENDF/B VIII [89], JENDL [90] and CENDL [91], include evaluations of cross sections and distributions of secondaries for key reactions based on a combination of measurements and estimates from nuclear model codes. They cover all measured interactions, from inelastic and capture at low energies; through inelastic interactions resulting in the emission of one or two neutrons (plus gammas); to multi-neutron production at tens of MeV. For some elements, data is available for several individual isotopes, while for others only the values for the natural composition are measured. Cross sections have many resonances in the keV–MeV region, complicating precise treatment.

For reactions that result in more than two outgoing particles, in most cases only spectra are available; i.e. information on the correlations of products is not included. As a result, sampling secondaries for one interaction in a way that conserves energy and momentum requires complex algorithms and additional computation. This has recently been introduced in PHITS; other codes rely on uncorrelated sampling and conserve energy only on average.

This detailed treatment consumes significant CPU and memory, because the full set of cross sections for all isotopes of all elements is required. Variants of this approach are utilised in MCNP/MCNPX (the gold standard for neutron simulation) and in the GEANT4's NeutronHP package.

A simpler approach averages cross sections over chosen sets of nuclei and fixed bins of energy. This 'multi-group' approach provides savings in memory use compared with the detailed approach and is adopted in FLUKA, as the option for precise treatment of low-energy neutrons. Accuracy is determined by the number of sets of nuclei and of the intervals of energy—and also the choice of the grouping.

In addition to the purely electromagnetic interactions of charged particles, and the interactions of hadrons with matter, it is necessary also to simulate the interaction of electrons, positrons and gammas with nuclei which result in hadronic final states. These photo-nuclear and electro-nuclear interactions account for a small portion of the total cross-section of gammas or electrons, below one percent at its peak. Yet they are the only interactions that convert electromagnetic energy into hadronic final states in typical HEP experiments.

Models for photo-nuclear and electro-nuclear interactions are provided in all multi-particle codes discussed [92].

Given the diversity of hadronic interactions, there is a need to focus on essential aspects. What most influences the accuracy of the description of the energy response, energy resolution of calorimeters and missing energy for hadronic calorimeters?

For HEP applications (in particular calorimeters) some of the key features are:

- most energy is deposited by low-energy particles, and its spectrum is independent of the type of projectile particle [93];

- the production of π^0 particles and the fluctuation of the energy fraction in this channel which leads to prompt EM energy deposition plays a determining role in the resolution of calorimeters [94, 95]; these π^0 's can be the result of charge exchange or other hadron–nucleon collisions, or formed by the soft fragmentation, e.g. in the QCD string view of high energy reactions;
- the simulation of neutron generation, transport and interaction, which contribute to prompt and delayed signal, activation, and escaping energy;
- a component of missing energy (that influences the resolution) is the energy lost to nuclear breakup. The accuracy of the modeling of all hadronic reactions, but in particular the de-excitation stage, determines the quality of its simulation;
- the simulation of leading particles which determines the shower profile—the profile of energy deposition—and in particular the sharing between longitudinal compartments and the amount exiting in the direction of the projectile.

The accuracy of the modeling of the time dependence of different interactions, both in a tool and in an experiment simulation, are also essential.

The fluctuation in the fraction of energy going into each type of secondary particle (gammas, charged hadrons, neutrons, neutrinos) in all reactions is an essential feature of a simulation tool. It is important for predicting and modeling the resolution and other aspects of detector performance.

11.3.11 From Full to Parameterized ('Fast') Simulation

In order to obtain high statistics, it is necessary for some applications to utilize simulation which is much faster (typically by two orders of magnitude) than the detailed full simulation. There is a spectrum of such simulations with different approximations and compromises.

The coarseness of simulation, from detailed to fast, is determined by a number of variables: whether the geometry is described approximately or in great detail; whether secondary particles are generated from the interaction of primary particles; the degree to which particles are eliminated during tracking—for example, the relation between the energy of primary particles and an energy threshold; and the type of physics models utilized. Choosing the least level of detail and following only the primary tracks distinguishes the fastest simulation. In other variants, some aspects are simulated in more detail in order to obtain more precision. Different ways can be used: simulating more particles, adding physics or geometry volumes.

In the first two LHC runs, it has been possible to produce billions of simulated events using detailed simulation. In some experiments the forward sub-detectors were simulated faster, e.g. use by ATLAS of frozen showers for forward calorimeters. Projections for the High Luminosity LHC era foresee an order of magnitude gap between the statistics possible using GEANT4-based detailed simulation on projected 2025 hardware and the needs of most analyses. This gap is driving the continued development of fast simulation methods, and the research into methods

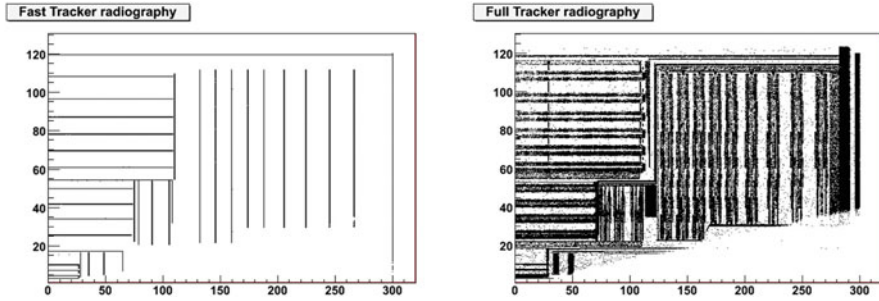


Fig. 11.1 Simulated radiography of a quarter of the CMS tracker geometry using the fast simulation FastSim (left) and full GEANT4-based simulation (right). This demonstrates the simplification of the geometry description used in fast tracker simulation, which projects the material onto smaller cylindrical shells, yet reproduces the hit structures and reconstructed tracks with the accuracy required in physics analyses. (Reproduced from [97])

for speeding up particle transport simulation. The GeantV [7] R&D aims to produce a prototype to demonstrate whether the core simulation work can be redesigned for more efficient use of current and forecast computer architectures with complex CPUs and deep memory architectures, with the goal of a speedup factor between 2 and 5.

The fastest type, so-called ‘parametric’ simulation involves the simplified propagation of tracks coupled with a reconstruction of fixed efficiency and idealized EM and hadronic calorimeters are given an input resolution. In one modern incarnation, Delphes [96], it is coupled with built-in reconstruction, and can be used to obtain first level estimates for some physics analyses from a simplified model of a detector. This type of simulation is used in the first feasibility stages of detector design, and to obtain a first understanding of physics analyses.

A more accurate type of fast simulation uses a simplified geometrical setup of a tracker device and/or sampling of showering using a parameterized distribution of a calorimeter to generate energy deposition hits and reconstruct events using about 100 times less computing resources than the full detailed simulation. An example of the simplified tracker geometry can be seen in Fig. 11.1, where the geometry of the CMS fast and full simulation of the tracker are compared.

The detailed geometry and physics of the full simulation, e.g. using GEANT4, is typically used as a yardstick for comparison of relevant physics quantities required by physics analyses, and sometimes to generate a library of pre-simulated showers at set energies for use in recreating realistic showers.

The LHC experiments have developed many different types of fast simulation, both specific to one part of a detector (tracker or calorimeter), and spanning the full detector.

One example is the mixing of detailed simulation for parts of the detector with simplified treatment within fixed regions or regions that depend on the particles inside an event or collision.

Recently ATLAS has produced an integrated simulation framework ISF [98], which includes detailed simulation and per-subdetector fast simulations. This enables the use of common modules for all elements of the simulation. A hybrid simulation mode is part of its design that selects conical regions around the most energetic primary particles for detailed simulation, and uses fast simulation models for the remaining parts of the detector. This capability has not yet been used in physics analyses.

11.4 Machine Learning for Fast Simulation

A completely new approach to parameterized simulation has emerged recently, exploring the potential of machine learning. One research avenue attempts to generate patterns of energy deposition that reproduced the distributions including fluctuations of key physical observables.

This has been the topic of interest and recent investigations using the generative-adversarial network (GAN) approach to the fast generation of patterns of hits. A first demonstration in a three layer LAr sampling calorimeter [99] was tested over an energy range from 1 to 100 GeV and a single particle direction. A potential speedup of $O(100)$ – $O(10,000)$ was demonstrated. Most physical observables of interest for the classification and calibration of tracks were well reproduced, but a few showed clear differences. This promising avenue will clearly be an area of significant research in the next years.

11.4.1 Accuracy of Simulation

The accuracy of the simulation is determined not only by the artificial differences or defects introduced by such simplifications, but also by intrinsic factors. These factors include the accuracy of the cross-sections for particular interactions and the capability of the physical models. These can be explored by comparing with experimental data.

Criticisms of detector simulation focus on key limitations and question the predictive power of hadronic interaction modeling for use in designing and tuning hadronic calorimeters [100].

11.4.2 Signal Generation

In order to model the signal produced in a gaseous detector, all processes that contribute to the generation of charge and its collection in the cathode must be simulated. The detailed simulation of a small number of events modeled in full detail is used to understand the characteristics of a detector. For large-scale simulation, a

simple model or parameterization is produced for the signal generation given the energy deposition.

The simulation involves a level of detail beyond other Monte Carlo simulation for HEP detectors. Some of the important aspects include:

- modeling the generation of all secondaries, without an energy threshold, in every single inelastic collision in the gaseous volume;
- the effects of elastic collisions in the transport;
- for efficiency, pre-calculating the convolution of the effects of the resulting diffusion and the drift in the electromagnetic fields of the detector;
- the effect of potential build-up of charge on detector elements, e.g. the space charge in a gas.

Due to the need to simulate down to the eV scale, this simulation requires detailed knowledge of the excitations of the molecular constituents of the mixture. Specialised programs are necessary for this simulation. Garfield calculates the electric field in many regular cell geometries. Then it combines it with the energy deposition for each atomic shell via a specialized Photo Absorption Ionization model integrated from Heed [101] to generate all secondary gammas and electrons. Transport of the charged particles in the electromagnetic field is coupled with diffusion, using pre-calculated transport coefficients generated by the Magboltz code [102].

It is possible to simulate an avalanche near a sensor wire in order to accurately model the signal arriving at the detector's electronics. This is typically required only for the detailed understanding of the effects of the shape of the signal and the integration characteristics of the electronics, and requires three orders of magnitude more computation than the simulation of the energy deposition in the gas volume. Alternatively, a fraction of the track can be simulated, in order to determine key characteristics, such as the arrival time of the signal. This reduces the computing requirements by about an order of magnitude.

It is also possible to calculate the effect of charged particles on an integrated circuit element [103]. Using the energy deposition to create electron-hole pairs, an external Technical Computer Aided Design (TCAD) program simulates the detailed response of the circuit. Applications of this technique have focused on the simulation of single event upsets [104], in which a cosmic ray track results in the flipping of a bit in a silicon circuit. Typically, the circuit response involves proprietary TCAD programs.

11.4.3 Production Thresholds and Other Biasing Techniques

For many setups, computing resources for simulation in full detail are not available. For example, large-scale experiments can require millions of events in order to establish patterns related to rare processes, yet the full simulation of events is prohibitive. In this case the choice must be made how to discard particular tracks in

order to achieve the required computing time per event, while influencing the most important results as little as possible.

The simulation time for each particle type is proportional to the number of steps, and typically the energy of a particle (so long as it does not escape the setup). The large number of electron and gamma particles in an EM or hadronic shower necessitates that these tracks are key to reducing the computation time. For this, either the treatment of each track must be simplified, or the average track length must be greatly reduced, or the number of particles tracked must be reduced. The use of a tracking cut reduces the average track length, and the use of a production threshold reduces the number of tracks simulated.

A number of methods are widely practiced to reduce the computing time by simulating only the more important particles: to generate only particles whose energy is above a threshold energy (production threshold); to kill tracks once they fall below an energy threshold (tracking cut), or to treat neutrons via their average cross section (multi-group).

In other setups the interest is to estimate the fraction of particles passing through or around a shielding barrier, which e.g. could stop all but one particle in a million. In such cases, a method to speed up the simulation is needed. To estimate the flux of particles passing through such a barrier the transport mechanics must be changed. Most changes will favor paths which have already crossed part of the barrier or are likelier to cross—e.g. because they have higher energy [105]. There are many methods to achieve this, all of which assign a weight to a particle track. Most involve the creation of extra copies of tracks or the killing of tracks. Some of the most common are importance biasing; leading particle biasing and weight window.

Importance biasing involves separating the geometry into regions of high and low numerical importance. At the boundary between such regions particles that go from low importance to high importance are enhanced in number (splitting), and their weight is reduced in proportion. Particles moving in the opposite sense are reduced in number (Russian roulette) and each one's weight is increased.

Leading particle biasing involves sampling the results of an interaction, favoring particles that have the highest energy (and most chance to penetrate) while sampling other particles in a representative way. In all cases surviving particles from populations, which are suppressed, are given higher weight in proportion to the difficulty of survival. On the other hand, enhanced particles (where two particle tracks are created from a single one) are given reduced weight. A single event can be split into a large number of 'histories', trial tracks that carry a different weight. Physical observables must be estimated accounting for the weight of a track—which can be interpreted as a probability:

$$\langle O \rangle = \frac{1}{N} \sum w_i O_i$$

The mean value of an observable O when using event biasing is calculated using the weighted sum of the values for each particle track 'history' i , which contributes, and the total number N of events (or trial histories).

11.5 Case Studies

The discovery of the top quark [106, 107] involved detector simulation only in a minimal and indirect way. Detector simulation was undertaken by CDF and D0 in the optimization phase of the design of their detectors. In D0 it informed the design of the interface between the central and end calorimeters [108]. Subsequently, simplifications were made for the detector simulation used in production, to reduce the computing time per event. The individual calorimeter plates were replaced by a large block, which contained a mixture of the absorber and active material. Optionally the response of particles below 200 MeV was parameterized. Comparisons with test beam determined that the full detailed plate setup agreed well; the simplified mixture setup was found to agree less well with test beam measurements, but judged adequate for most purposes.

Events simulated using the D0 simulation program were used in the later observation of the production of single top quarks [109]. However, the detector simulation was found to have significant limitations; these appear to have stemmed both from the simplifications of the modeling of the detector and its response and from the intrinsic limitations of the simulation tool. Several corrections were required, including a factor for the efficiencies of the trigger reconstruction, and for the efficiency to identify and select particles and jets.

In the LHC experiments, simulation was first utilized to model the response of the calorimeters to muon, electron and hadron beams. One key application has been the detailed calibration of the energy response of the electromagnetic calorimeter, to obtain an estimate of the energy of the incoming particle as a function of the inferred visible energy measured as signal in the different calorimeter compartments.

The ATLAS calorimeter system is complex, utilizing different detector materials, geometrical structure and technologies for the different rapidity regions. The insensitive material between parts of a detector distorts the energy signal due to tracks crossing this region. Simulation is used to obtain correction factors for the energy of the incident particle or jet.

ATLAS has undertaken an extensive comparison of test beam results with Monte Carlo simulation. Simulation utilising GEANT 3.21 in the 1990s was used for detector design studies and the first test beam comparisons. Progressively from 2000 onwards, test beam results were compared mostly with GEANT4, and in 2004 a Geant4-based simulation was declared the official ATLAS ‘production’ detector simulation in 2004.

Comparisons were undertaken first with the test beam results for individual detectors. A typical comparison started with muons, as minimum ionizing particles, to make a first verification of the material description and geometry of active parts. Next, measurements of electrons were compared, verifying the detector description of passive parts. This determines the factor for conversion of the deposited energy into the signal measured by each detector, its electromagnetic scale, by comparison with a beam of a particular energy, typically 100 GeV. Key

observables compared include the linearity of the response, the energy resolution and the shower longitudinal and lateral shapes.

The comparisons identified areas where improvement was necessary: there were problems in the large dependence of the electron energy response on the production thresholds. These were also reported in studies related to the use of GEANT4 in medical applications [110] and were corrected in GEANT4 release 8.0.

11.5.1 Calibration of EM Calorimeter Using Monte Carlo

The calibration of the ATLAS liquid argon (LAr) Electromagnetic Calorimeter for electrons was developed utilizing a detailed Monte Carlo simulation of the detector and its test beam [111]. The simulation included a very detailed description of the complex geometry, collection of the energy deposition into hits and conversion to digitized signal.

The simulation was shown to describe well all the relevant measurements, including the mean reconstructed energy, the distributions of energy deposition in particular compartments and the energy profiles in the longitudinal compartments and lateral sections. For example, the mean reconstructed energy was described to within 2% in the Pre-Sampler and the first two (of three) compartments of the accordion. Also the distribution of the total reconstructed energy is described very well—within the uncertainty due to the upstream material ahead of the setup and in front of the PreSampler.

Based on this agreement, the simulation was used to correct for several effects, which could not be measured or could only be estimated indirectly. One involved the average energy deposited in the dead material between the pre-sampler and the first compartment; this provided an estimate of this energy deposit. Another effect was Bremsstrahlung in upstream material, due to which a fraction of events arrives at the detector with reduced energy. A quantitative description was made and compared with the measured total energy deposit.

Dedicated Monte Carlo simulations were undertaken to study the systematic uncertainties induced by each effect. As a result, the reconstructed energy response in the energy range from 15 to 180 GeV was found to be linear within 0.1% (an exception is at 10 GeV, where it was found to be 0.7% lower). The systematic uncertainties due to incomplete knowledge of the detector, the test beam, or the reconstruction were found to be about 0.1% at low energies and negligible at high energies. The effect of the non-linearity at about 40 GeV and above on the measurement of the W^+/W^- mass was found to match the aimed precision of 15 MeV—provided it can be extended from the section tested to the full calorimeter.

11.5.2 *Hadronic Calorimeters: Comparisons with LHC Test Beam Results*

For the hadronic calorimeters, after muons and electrons, the test beam results with pions were compared to simulation. This served to validate the simulation of hadronic interactions, since the conversion of the energy deposition into signal is common with the electron test beams. Additional observables compared included the longitudinal and lateral shower shape.

The ATLAS Hadronic Barrel Calorimeter's (TileCal) use of scintillator requires the accurate simulation of neutrons for those interactions that contribute significantly to energy deposition and which occur within its time window of 150 ns. This is treated in the simulation.

ATLAS has also undertaken extensive test beam measurements of the response of the TileCal to pions. The most recent comparisons in the Combined Test Beam setup (2004) involved pion energies up to 350 GeV. These tests [112] examined the energy response and resolution of the calorimeter, and compared them with the predictions of a simulation based on GEANT4 (version 9.1).

Events were selected based on several criteria, including the energy deposition in a cryostat scintillator (SC1) placed before the TileCal. This cut was made in order to enable comparisons with the previous test beam. Potential biases from this selection cut on the response and resolution were studied. An approximation of this cut was used in the simulation: the energy deposition in the surrounding dead material. The change in the energy response due to this cut ranged from -2.5% to $+0.5\%$ depending on the energy and eta value (0.25–0.65) of the pion beam. This was reproduced within 0.5% at low energy (20 GeV) and within 1.5% at high energy (300 GeV).

The energy resolution was affected in a range from $+10\%$ to -10% between low and high energies respectively and reproduced within 2% for a large combination of angles and energies, except for a 4% deviation at one angle at 20 GeV. Comparing the final results for the energy response, the agreement obtained is within 3% for the full energy range studied (20–350 GeV). Typically, agreement at the 1–2% level is achieved for beam energies of 50–250 GeV; greater deviations are seen at 20 and 300 GeV (the latter, in particular, remains to be understood). For the energy resolution agreement at the 10% level is obtained.

The measurements of the reconstructed energy in the Atlas TileCal at energies from 20 GeV to 180 GeV have also been compared with simulation [113]. Figure 11.2 shows the ratio of simulation and data for the energy for the case of incident pions using different configurations of physics models in 2010 with GEANT4 version 9.2. Agreement for the mean energy between simulation and data ranges from -10% (the legacy LHEP physics modeling) to $+3\%$ (the production physics list QGSP_BERT). The root mean square deviation (RMS) of the reconstructed energy agrees within -4% (QGSP_BERT) to about $+15\%$ (LHEP).

Since a 1 MeV neutron could travel only 3 cm within 100 ns, even if it never interacted, the propagation of low energy neutrons—and thus their contribution to

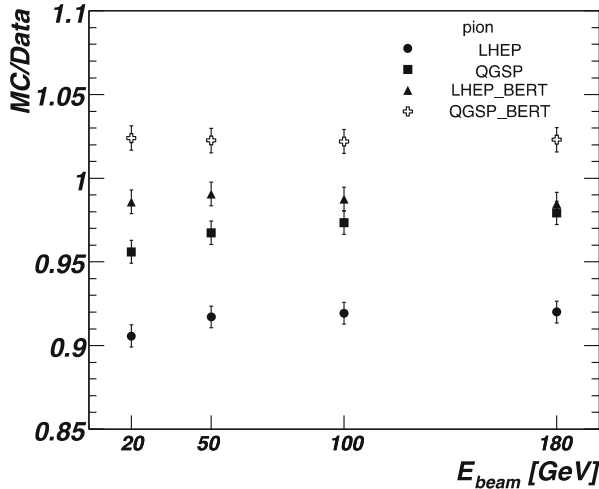


Fig. 11.2 Comparison of the reconstructed energy in the ATLAS Tile calorimeter (TileCal) with several different physics models. The ratio of the simulated (MC) response with the response reconstructed from test beam runs (Data) for pions of energies from 20 GeV to 180 GeV. GEANT4 9.2 was used, comparing the predictions of different physics lists. The normalization uncertainty is 1%. (Courtesy of the Atlas Collaboration. Reproduction with permission)

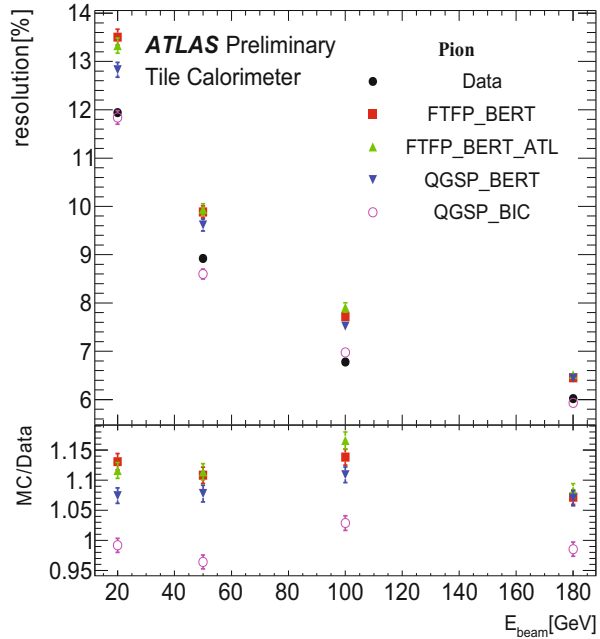
the signal—is limited to short distances near the point of their generation during the typical trigger window of an LHC detector.

Comparing with the same Tilecal test beam, with the beam at 90 degrees with different physics lists of release 10.1, the version used for Run 2 simulation by ATLAS, demonstrates the change in physics performance from the revision of physics modeling in GEANT4. The energy resolution (Fig. 11.3), longitudinal shape (Fig. 11.4) and lateral shapes (Fig. 11.5) are compared with four physics lists that combine the QGS or Fritiof FTF string models with the Bertini or Binary cascade.

11.5.3 Background Estimation for CMS

Simulations were used to assess the required shielding for the CMS detector, to reduce the background from the interaction region p–p collisions [33] and the accelerator tunnel [114]. These employed a combination of tools: the STRUCT code was used for simulation the accelerator lattice and the scoring of particles lost at collimators, MARS to generate the particles entering the experimental area and FLUKA to model their interactions and fluxes in the detector and surrounding area. The study confirmed the need for shielding from the accelerator background and evaluated the proposed solutions. Key aspects were the impact on muon physics, together with the flexibility of optionally tracking the products of muon-

Fig. 11.3 Energy resolution of ATLAS Tilecal test beam compared to recent GEANT4 10.1 release, currently used in ATLAS simulation production. Lower panel is the ratio of simulated (MC) and data. Courtesy of the ATLAS collaboration (ATLAS public plot). The original data and comparisons of mean and RMS energy [113] were undertaken with GEANT4 version 9.2



nucleus interactions. The study identified high-energy muons as the most important remaining background, affecting, in particular, the innermost barrel chambers, contributing to approximately 10% to the total trigger rate (which is very small).

11.5.4 Validation from Comparisons with In-Situ Data

The accuracy of the simulation is determined using selected in-situ data from collisions, whenever possible. For example, ATLAS selected proton–proton collisions at 7 TeV (2010) and 8 TeV (2012) [115] to compare the energy deposition of charged hadrons with energies up to 30 GeV.

Decays of Λ , anti- Λ and K_s^0 were used to identify π^+ , π^- , protons and antiprotons and the ratio of their measured energy and momenta were compared with simulation using GEANT4 version 9.4. The ratio of Λ and anti- Λ to K_s^0 is 40% higher in data than in simulation, but the normalized distributions are well reproduced within statistical precision, as seen in Fig. 11.6. The tail beyond $E/p > 1$ is due to the neutral background. The fraction of $E/p \leq 0$ is due to interactions before the calorimeter; it is underestimated about 10% by the simulation across all particle species. The difference is taken between particle species of the mean values of E/p in order to reduce the effect of the neutral background. The difference between π^- and antiprotons, due to extra energy from the antiprotons annihilation, is described within uncertainties by the FTFP_BERT physics list in GEANT4 version 9.4.

Fig. 11.4 Longitudinal shower profile of 50 GeV pion and 180 GeV proton beams in ATLAS Tilecal, with the modules placed at 90 degrees in dedicated test beam setup, versus recent GEANT4 10.1. Lower panel is the ratio of simulated (MC) and data. Courtesy of the ATLAS collaboration (ATLAS public plot). The original data and earlier comparisons (vs. GEANT4 ver. 9.2) were in Ref. [113]

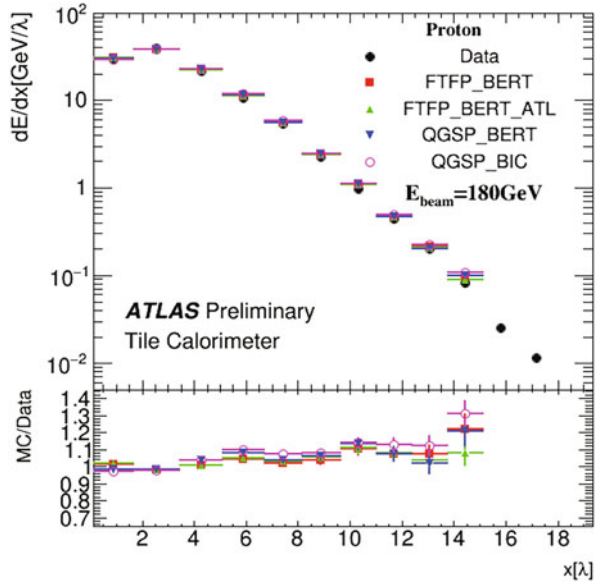
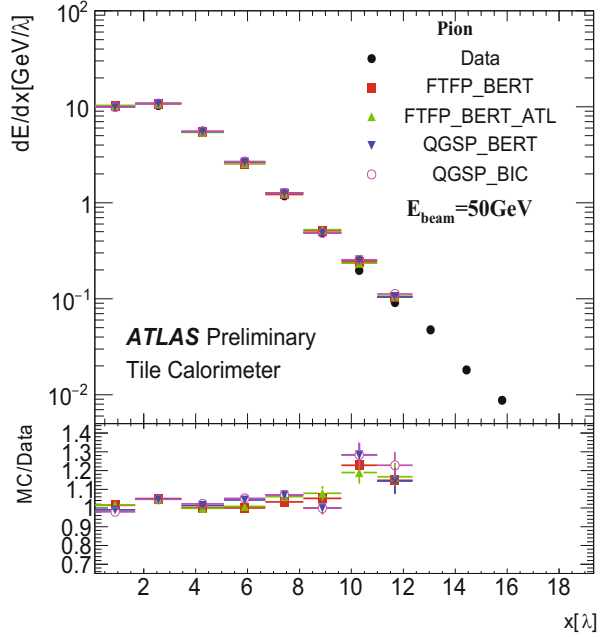
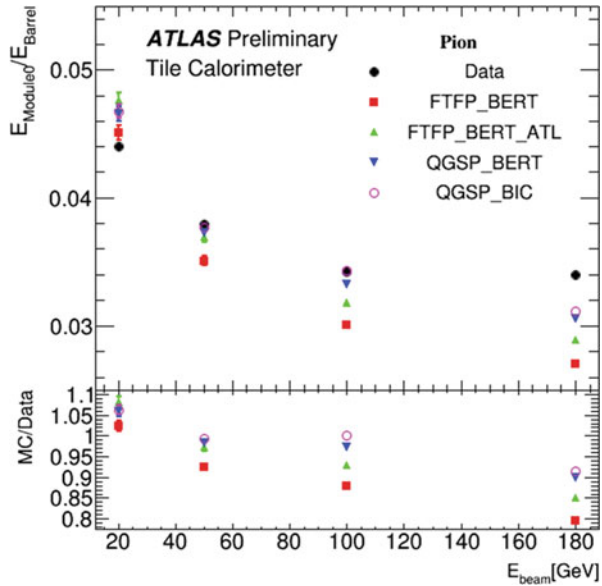


Fig. 11.5 Lateral spread of 20, 50, 100 and 180 GeV pions incident on the ATLAS Tile Calorimeter at 90-degree angle. Black points represent data obtained in the period 2000–2003, and the colored points simulations using different physics lists of GEANT4 version 10.1. Lower panel is ratio of simulated (MC) and data. Courtesy of the ATLAS collaboration (ATLAS public plot). The original publication [113] compared data with the earlier version 9.2 of GEANT4



Inclusive spectra of isolated hadron tracks were used to compare E/p distributions with simulation. After the energy deposition of neutral particles is subtracted, a 5% discrepancy was found in the response to isolated charged hadrons between the modelling using two GEANT4 hadronic physics lists (FTFP_BERT and QGSP_BERT) in the central region of the calorimeter (Fig. 11.7).

When tracks that interact only in the hadron calorimeter were examined separately, the detector simulation was found to describe the response well. Tracks that interacted only in the EM calorimeter showed discrepancies 5–10% in E/p , which is consistent with being the origin of the difference of all tracks.

These comparisons are used in one of the methods of estimating the uncertainty of the jet energy scale. Compared with the most recent estimations of the jet energy scale, these estimates have larger uncertainties over most of the energy range, but confirm estimates from in situ beam data. However, they currently provide the only estimate for the largest momenta ($p_T > 2$ TeV).

11.5.5 The Estimation of Jet Energy Scale in ATLAS and CMS

The earliest estimates of the jet energy scale, in the first years of the operation of ATLAS and CMS relied critically on detector simulation.

In CMS the detector simulation using GEANT4 was used in multiple stages of the initial calibration of the jet energy scale [116]. Initially, it was used to determine a base calibration factor $C_{MC}(p_T^{\text{reco}})$ to account for the fraction of jet energy not

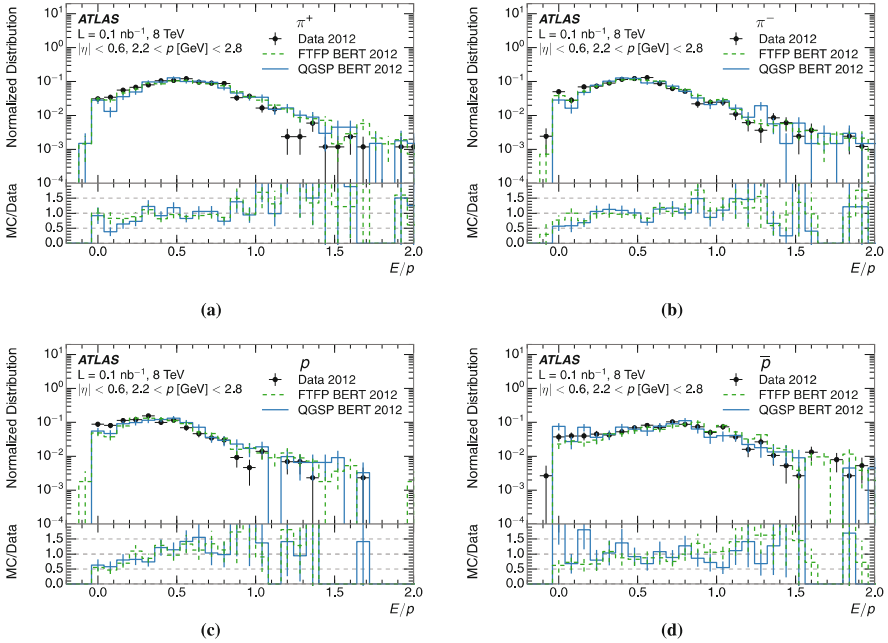


Fig. 11.6 The E/p distribution for (a) π^+ , (b) π^- , (c) protons and (d) antiprotons from selected ATLAS 8 TeV data of identified Λ , anti- Λ and Ks decays [115] with $|\eta| < 0.6$ and $2.2 < p[\text{GeV}] < 2.8$. The lower part of each panel shows the ratio of MC simulation (using GEANT4 ver. 9.4) to data. Reproduced from [115] under the Creative Commons License 4.0

observed due to the inactive parts, and to determine the variation of response for different types of particles.

Subsequently, the balance of the transverse momenta of $\gamma + \text{jets}$ and $Z + \text{jets}$ events was used to compare the well-measured electromagnetic response to the hadron/jet response predicted by simulation for different p_T and η values. CMS concluded that the Monte Carlo correction factor described the bulk of non-uniformity of C_{MC} in η and non-linearity in p_T . The estimates of the data/MC ratio of jet energy using the different samples (Fig. 11.8) were consistent, flat in p_T and its value was $R_{\text{data}/MC} = 0.985 \pm 0.001$.

The estimation of the jet energy scale with Run II data relies less on simulation. Comparisons versus simulation based on a newer GEANT4 version (10.2) found that a larger correction was required, partially ascribed to the migration to Fritiof-based hadronic models.

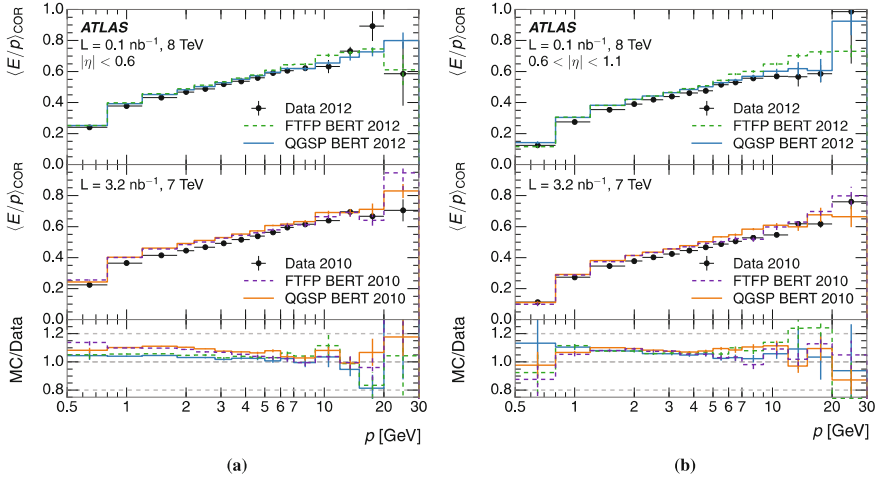


Fig. 11.7 Comparison of the average ratio $\langle E/p \rangle_{\text{COR}}$ of charged tracks of cluster energy in ATLAS calorimeters versus momentum p measured in the tracker. Comparisons within (a) $|\eta| < 0.6$, and (b) $0.6 < |\eta| < 1.1$, obtained after subtraction of corresponding estimates of neutral particle response, versus track momentum. Tracks with no matching energy cluster in the calorimeter are included. The bottom portion of the panels shows the ratio of simulation (using GEANT4 version 9.4 and two physics lists) to data. Error bars are statistical. Reproduced from [115] under the Creative Commons License 4.0

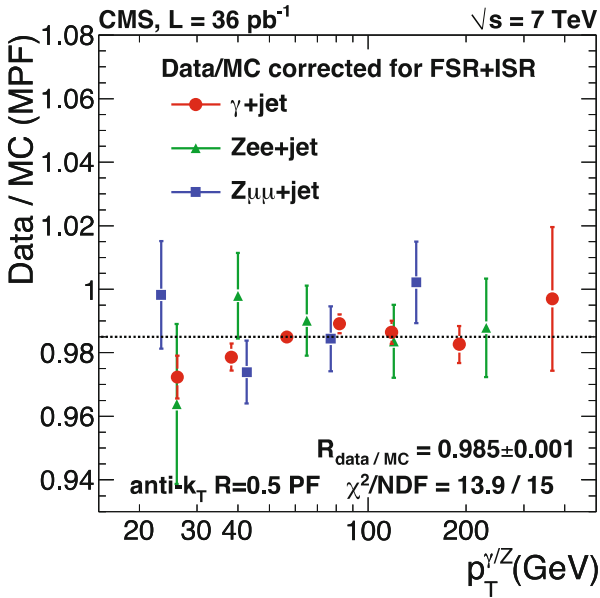


Fig. 11.8 Correction factor from comparison of $\gamma/W + \text{jet}$ events in CMS 2010 data at $\sqrt{s} = 7 \text{ TeV}$. From Ref. [116], reproduced under the Creative Commons license 3.0

11.5.6 Fast Simulation in CMS During LHC Run I and II

The fast simulations of the LHC experiments are sophisticated programs, combining the most important physics processes for electrons, gammas in the trackers and muons in the muon systems, with sampling from parameterized distributions for the showering of electrons, gammas and hadrons in the calorimeters. CMS's fast simulation FastSim [117] is a simplified geometrical description of the tracker, refined to obtain percent-level agreement for photon conversion, using around 30 thin nested cylinders.

The fast simulation in the tracker reconstructs each track using only its own generated hits, and cannot reproduce fake tracks that result from the incorrect association of hits. Though good agreement is seen in comparisons with Run-I data, the limitations of this approach are apparent in modeling the efficiency of track reconstruction and the fake rate [97].

Electron and hadron showers in calorimeters are turned into energy spot hits directly, distributed according to a Γ -function with parameters which fluctuate between showers using GLASH [118] or a similar approach.

Regular comparisons with the full detector simulation are used to monitor all the quantities used in physics analyses [119]. Agreement is observed at a level of 10%. Good agreement is particularly important for the missing transverse energy E_T .

During Run-I the CMS FastSim was used for the parameter scans for SuperSymmetry searches and samples of events used to evaluate systematic uncertainties [97], because the computing resources required for full simulation would have exceeded the available ones.

Once in-situ data is available, they are used as the final yardstick of the quality of both the fast and full simulation, and are used to address possible discrepancies between fast and detailed simulation.

11.5.7 Future Detectors: Fine-Grained Calorimeters of CALICE

Proposed detectors for next-generation collider experiments rely on particle flow reconstruction methods to obtain the required energy resolution for their physics programme. In order to obtain this performance, it is necessary to accurately model the energy deposition of charged hadrons, in order to subtract them from the observed signals.

Measurements with fine-grained calorimeters provide the most promising methods to validate the most important properties of detector simulation tools, and in particular their hadronic modeling. The CALICE experiment has undertaken test beam measurements of prototype calorimeters with many layers of scintillator tiles of fine granularity.

The prototype calorimeter with analog readout consisted of 38 layers, each containing a steel absorber plate and a scintillator layer. The $30 \times 30 \text{ cm}^2$ core of the scintillator had granularity $3 \times 3 \text{ cm}^2$, and outer regions $6 \times 6 \text{ cm}^2$ and $12 \times 12 \text{ cm}^2$. Data was collected with pions between 8 GeV and 100 GeV and compared with Monte Carlo simulation [120] using GEANT4 version 9.4.

The fine segmentation allows the estimation of the layer of the first hard interaction. This is used to obtain the shower profile relative to this starting layer. Averaging over showers starting in different layers reduces the effect of the variation of calibration, and is used to estimate uncertainties.

Comparisons of the mean longitudinal and lateral shower profiles for 8 GeV, 18 GeV and 80 GeV pions with GEANT4 physics lists including QGSP_BERT and FTFP_BERT were provided.

Figure 11.9 top row shows the longitudinal shower profile for pions of 8 GeV (left), 18 GeV (center) and 80 GeV (right) compared with GEANT4 physics lists FTFP_BERT.

Normalization to unit total is used in each distribution. For FTFP_BERT less energy is deposited in the early shower layers at all energies. At 80 GeV a difference is seen in the shower maximum of 10% (FTF versions) to 20% (QSGP versions), and the shower is more compact.

Similar comparisons for the radial shower profile show that all physics lists underestimate the radial extent of the showers and have a larger fraction of energy in the core. The effect is most pronounced at 80 GeV, see Fig. 11.10.

Either improvement of the relevant models or alternative physics models is needed to better describe these shower shapes, and provide the accuracy to use the full potential of simulation for future highly granular calorimeters.

11.6 Applications in Other Fields

Particle transport simulation tools, including GEANT4 and FLUKA, have seen greatly increasing usage beyond High Energy and Nuclear Physics (HENP) experiments in the past decade.

In particular in medical physics, their application has seen spectacular growth, and has spanned several domains, especially the development and refinement of new methods and assessment of treatments in radiotherapy, and the simulation of medical imaging detectors.

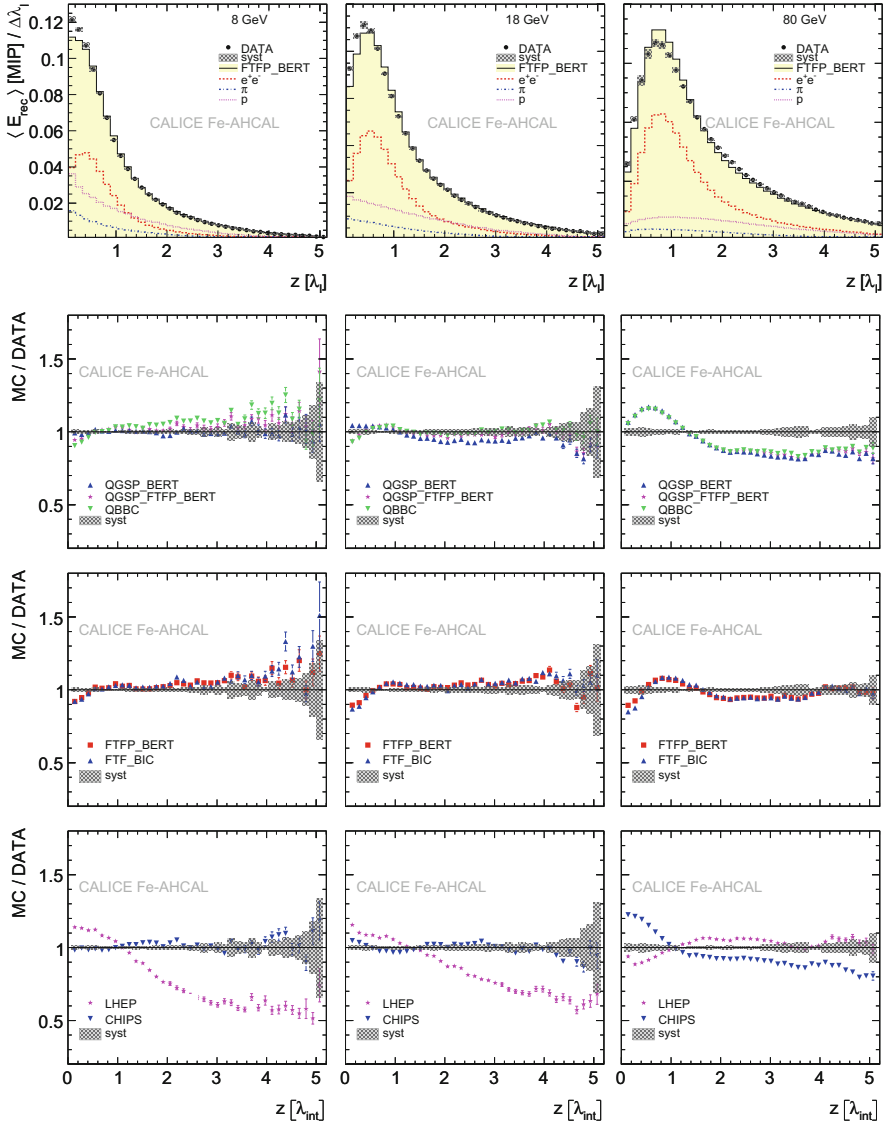


Fig. 11.9 Mean longitudinal shower profile, starting at the layer of the first interaction, for pion beams in CALICE iron-scintillator analog hadronic calorimeter. Pion energies are 8 GeV (left), 18 GeV (center) Top row: data (circles) compared with FTFP_BERT physics list of GEANT4 version 9.4. The parts deposited by different particles (electrons/positrons, pions and protons) in the simulation are shown. Lower 3 rows: ratios between selected physics lists and data. (We note that the CHIPS and LHEP physics lists were withdrawn in Geant4 release 10.0). Reproduced from [120], under Creative Commons License 3.0

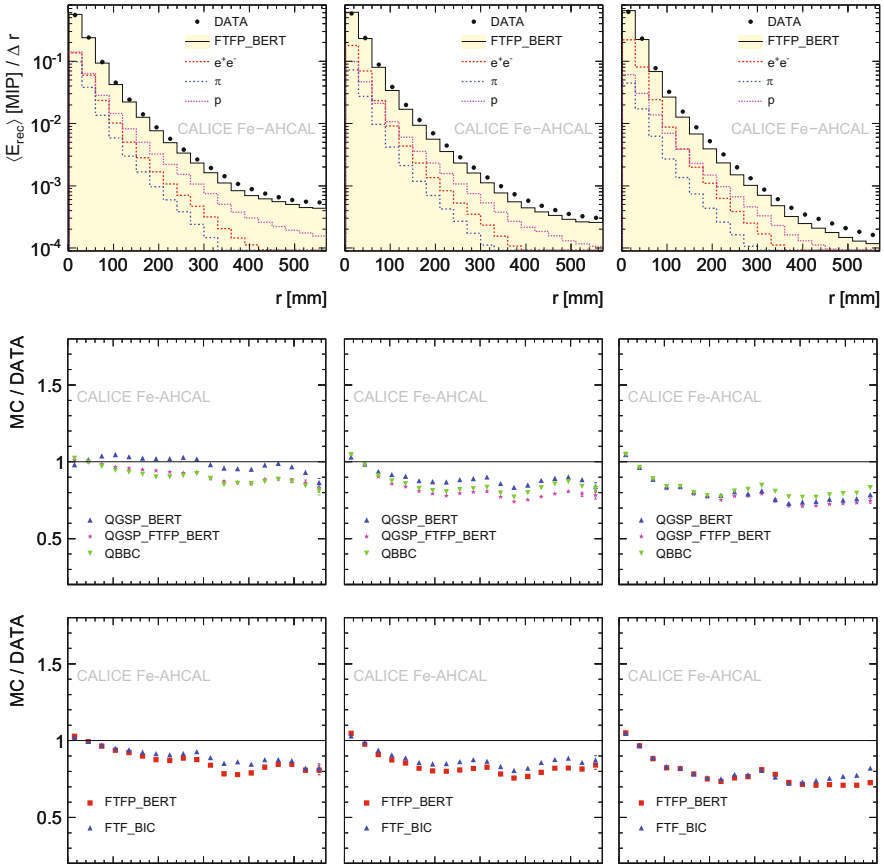


Fig. 11.10 Mean radial shower profile for pion beams in CALICE iron-scintillator analog hadronic calorimeter. Pion energies are 8 GeV (left), 18 GeV (center) and 80 GeV (right). Top row: data (circles) compared with FTFP_BERT physics list of GEANT4 version 9.4. Deposits by different particles (electrons/positrons, pions and protons) in the simulation are shown. Centre and lower row: ratios between selected physics lists and data, including QGSP_BERT and FTFP_BERT and variants. Reproduced from [120], under Creative Commons License 3.0. (Physics lists using models withdrawn in subsequent releases, CHIPS and LHEP, are omitted)

The simulation tools are used widely also in determining the effect of radiation on satellites and spacecraft from planetary radiation environments and the solar and galactic rays. Specialized tools have been developed for shielding studies [121] as have general purpose tools to evaluate effects of the space environments [122].

FLUKA is used for shielding and target design of accelerators, activation studies, and also for cosmic ray studies, due to its ability to simulate up to 20 PeV. A further application is the assessment of dose to aircrews flying in commercial aircraft.

11.6.1 Medical Imaging

A key application of Monte Carlo simulation in medical imaging is the development of novel instrumentation, e.g. progress in Position Emission Tomography (PET) and Single Photon Emission Computed Tomography (SPECT). Particle transport simulation enables an evaluation of new materials, geometries or system configurations in multiple versions without the expense of always creating a hardware prototype [123].

Dedicated particle transport tools have been developed specifically for the simulation of PET or SPECT devices. An early tool PET-EGS [124] used EGS, with GEANT4 used in the leading tool, GATE [125], and in GAMOS [126], and Penelope in PeneloPET [127].

GATE is one of the most commonly used dedicated simulation tools for PET [123]. This is due to its simplicity in generating setups and steering the simulation using text commands, and due to the benefits of the validation of the GEANT4 toolkit.

Particle transport simulation is a standard tool in many applications. However, one of its key drawbacks is the large computation times required. Methods have been therefore developed to mitigate this problem. As an example, networked computers are being employed to speed up the calculations. Alternatively, hybrid computational models are being employed, such as generating the initial photons using SIMSET [128] or using EGSrc as its core simulation engine [129].

11.6.2 Proton and Hadron Therapy

As in photon radiotherapy, the recent advances of proton and ion beam therapy have heavily relied on radiation transport Monte Carlo tools [130]. Due to the need for short computation time, specialized Treatment Planning Systems (TPS) with analytical or simplified models for the fast estimation of dose delivery are the clinical standard.

GEANT4 validation for proton-therapy involves selection of the best performing physics models [131]. These tools are also essential in evaluating potential improvements in TPS methods [132].

Another critical aspect is the simulation of the effects of organ motion on dose delivery, e.g. with the GEANT4-based GATE and standalone applications [133].

Specialized applications were developed to use GEANT4 in particle therapy and provide tailored and validated physics configurations, interfaces to CT input, and tools including the reading and writing of snapshots of particles at specific interfaces as phase space files. In the past decade two dedicated applications, PTSim [134] and TOPAS [135] targeted easy use by clinical physicists in Japan and the US respectively. TOPAS emphasized reliable configuration, and modelling of the motion

of components. Both have seen increasing use for research and in selected clinical settings.

The therapy potential of light ion beams has been the topic of increasing research during the past decade. A key drawback is the energy deposition of nuclear fragments which extends beyond the Bragg peak. Early comparisons identified discrepancies of some tens of percent in non-differential quantities between data and MC [136].

In more recent studies better agreement in these tail dose depositions and dose profiles was obtained with GEANT4 and FLUKA, but differences in prompt gamma emission continue to be an issue [137]. The lateral beam widening is also well confirmed by FLUKA results [138].

A key need in ion therapy is the monitoring of the range of ions. The detection of positron emission in a PET detector has been in clinical use, and a newer method involves prompt gamma emission. Both techniques have been investigated using particle transport to quantify the location of emission and the spectra of clinically interesting gammas.

Modeling of ion-ion interactions at therapeutic energies is frequently at the edge of applicability for cascade models (below 150–200 MeV), and the resulting spectra are influenced by the details of many nuclear de-excitation processes. Discrepancies in secondary particle production in FLUKA were improved with the addition of a Boltzman Master Equation (BME) model and other modelling refinements [139]. New measurements have been made with ion projectiles to provide data for comparison and improvement of modelling. One set using lower energy (62 A MeV) ^{12}C beam measured a large set of secondary spectra (p, d, t through to ^{11}B) [140]. Comparison with GEANT4 models revealed the need for improvement of the modeling used (binary cascade and QMD).

FLUKA's existing applications in particle therapy [141] include the production of data for Treatment Planning Systems (TPS), checking the plans created by TPS in selected cases for quality control and improvement of patient dose delivery, and in feasibility and sensitivity studies of prompt gammas for range and dose monitoring. Another use has been the monitoring of dose delivery in ion therapy through PET imaging of positron emitter production, undertaken either after treatment or through an integrated PET device during the patient treatment.

11.6.3 Developments for Microdosimetry and Nanodosimetry

New models and adaptation of physics models have been developed to extend their application to smaller energies. Dedicated Monte Carlo track structure codes have been used in the investigation of radiation effects at the micron scale and at scales appropriate for biological research [142] and modeling of radiotherapy outcomes [143]. GEANT4 has been extended to provide track structure modeling in liquid and gaseous water with the development of the GEANT4-DNA package [144]. This has enabled its use in many applications in these fields [145, 146].

The GEANT4-DNA package provides new physical models for the description of elastic and inelastic electromagnetic interactions of electrons and select ions (Li to O, plus Si and Fe) in liquid water, previously only available in dedicated ‘track structure’ codes such as PARTRAC [147]. In addition, GEANT4-DNA offers features to model the water radiolysis from ionizing radiation: ionized or excited water molecules and water anions are generated and tracked at a physicochemical stage up to a few picoseconds, and subsequently in a ‘chemical’ stage using models of generation, diffusion and reaction of new chemical species. This is part of an effort to model and understand the first stages of DNA damage.

11.7 Outlook

During the past decade the application of detector simulation tools has been significantly widened through the implementation of improved physics models. Code and models have become more accurate in describing benchmark data. The need for more accurate data for comparison and model improvement has been one motivation for some thin-target (HARP, MIPP) and thick target (CALICE) experiments.

The requirements that arise from the projected use of simulations as an integral part of the next generation detectors becomes ever stronger. Witness, e.g. the use of particle flow reconstruction [148] in proposed experiments at the energy frontier, including the Linear Collider and the Future Circular Collider, to address one of their major challenges.

The need for further development of physics models for high-energy hadron-nucleus interactions is evident. Several promising approaches are being pursued, including the extension and tuning of existing implementations of current models (Fritiof, Quark-Gluon String), the incorporation of alternative implementations of existing models, such as QGSJET, complementary modeling approaches (DPMJET) and the incorporation of new models (EPOS). The availability of high quality thin target experimental data at energies over a range of momenta from 20 to 158 GeV/c [149] is an important resource; lack of data for higher energies is a constraint.

In addition to physics improvements, the large increase in statistics of simulated events for the HL-LHC requires a large improvement in CPU performance, of approximately a factor of ten. Research in CPU-performance and emerging architectures in the GeantV R&D effort indicate a more realistic target of a factor of 2–4 in performance improvement may be within reach for detailed simulation.

These prospects strengthen the need for parameterized (fast) simulation methods which can reproduce the results of detailed simulation as accurately as possible, for use in a majority and potentially an ever-larger fraction of analyses. Hybrid methods combining parameterized and detailed simulation in innovative ways and the machine learning approach to parameterized/fast simulation appear amongst the options which will see significant development and research in the next years.

Bibliography

1. Graf, N., McCormick, J.: Simulator For The Linear Collider (SLIC): A Tool For ILC Detector Simulations. In: AIP Conference Proceedings. pp. 503–512. AIP (2006)
2. Frank, M., Gaede, F., Nikiforou, N. et al.: DDG4 A Simulation Framework based on the DD4hep Detector Description Toolkit. J. Phys. Conf. Ser. 664, 072017 (2015). <https://doi.org/10.1088/1742-6596/664/7/072017>
3. Behnke, T., Brau, J.E., Burrows, P.N. et al.: The International Linear Collider Technical Design Report - Volume 4: Detectors. Batavia, IL (United States) (2013)
4. Daniel Elvira, V.: Impact of detector simulation in particle physics collider experiments. Phys. Rep. 695, 1–54 (2017). <https://doi.org/10.1016/J.PHYSREP.2017.06.002>
5. Albrecht, J., Alves, A.A., Amadio, G. et al.: A Roadmap for HEP Software and Computing R&D for the 2020s. (2017). <https://doi.org/10.1007/s41781-018-0018-8>
6. Alves, A.A., Amadio, G., Anh-Ky, N. et al.: A Roadmap for HEP Software and Computing R&D for the 2020s. (2017)
7. Amadio, G., Apostolakis, J., Bandieramonte, M. et al.: The GeantV project: Preparing the future of simulation. J. Phys. Conf. Ser. 664, (2015). <https://doi.org/10.1088/1742-6596/664/7/072006>
8. Sjöstrand, T., Ask, S., Christiansen, J.R. et al.: An introduction to PYTHIA 8.2. Comput. Phys. Commun. 191, 159–177 (2015). <https://doi.org/10.1016/j.cpc.2015.01.024>
9. Andersson, B., Gustafson, G., Pi, H.: The FRITIOF model for very high energy hadronic collisions. Zeitschrift fr Phys. C Part. Fields. 57, 485–494 (1993). <https://doi.org/10.1007/BF01474343>
10. Sjöstrand, T., Bengtsson, M.: The Lund Monte Carlo for jet fragmentation and e+ e- physics - jetset version 6.3 - an update. Comput. Phys. Commun. 43, 367–379 (1987). [https://doi.org/10.1016/0010-4655\(87\)90054-3](https://doi.org/10.1016/0010-4655(87)90054-3)
11. Corcella, G., Knowles, I.G., Marchesini, G. et al.: HERWIG 6: an event generator for hadron emission reactions with interfering gluons (including supersymmetric processes). J. High Energy Phys. 2001, 10 (2001)
12. Bellm, J., Gieseke, S., Grellscheid, D. et al.: Herwig 7.0/Herwig++ 3.0 release note. Eur. Phys. J. C. 76, 196 (2016). <https://doi.org/10.1140/epjc/s10052-016-4018-8>
13. Agostinelli, S., Allison, J., Amako, K. et al.: Geant4—a simulation toolkit. Nucl. Instruments Methods Phys. Res. Sect. A Accel. Spectrometers, Detect. Assoc. Equip. 506, 250–303 (2003). [https://doi.org/10.1016/S0168-9002\(03\)01368-8](https://doi.org/10.1016/S0168-9002(03)01368-8)
14. Nakao, N., Mokhov, N.V.: MARS15 code in accelerator applications. <http://www-ap.fnal.gov/users/mokhov/papers/2007/Conf-07-416-APC.pdf> (2007)
15. Brun, R., Giani, S.: GEANT—Detector description and simulation tool. (1994)
16. Fesefeldt, H.S.: Simulation of hadronic showers, physics and applications. Physikalisches Institut, RWTH Aachen Physikzentrum, 5100 Aachen, Germany (1985)
17. Zeitnitz, C., Gabriel, T.A.: The GEANT-CALOR interface and benchmark calculations of ZEUS test calorimeters. Nucl. Instr. Methods A. 349, 106–111 (1994). [https://doi.org/10.1016/0168-9002\(94\)90613-0](https://doi.org/10.1016/0168-9002(94)90613-0)
18. Gabriel, T.A., Bishop, B.L., Brau, J.E.: The physics of compensating calorimetry and the new calor89 code system. IEEE Trans. Nucl. Sci. 36, 14–22 (1989). <https://doi.org/10.1109/23.34394>
19. Fassò, A., Ferrari, A., Ranft, J., et al.: FLUKA: present status and future developments. In: Menzione, A. and Scribano, A.P.G. 493 (eds.) Proc. IV Int. Conf. on Calorimetry in High Energy Physics, La Biodola, Italy, 21–26 Sept. 1993. p. World Scientific. World Scientific (1993)
20. Battistoni, G., Boehlen, T., Cerutti, F. et al.: Overview of the FLUKA code. Ann. Nucl. Energy. 82, 10–18 (2015). <https://doi.org/10.1016/J.ANUCENE.2014.11.007>

21. Roesler, S., Engel, R., Ranft, J.: The Monte Carlo Event Generator DPMJET-III. In: A. Kling M. Nakagawa L. Távora & P. Vaz PG - 1033, F.B. (ed.) *Advanced Monte Carlo for Radiation Physics, Particle Transport Simulation and Applications*. p. 1038 (2001)
22. Allison, J., Amako, K., Apostolakis, J. et al.: Recent developments in Geant4. *Nucl. Instruments Methods Phys. Res. Sect. A Accel. Spectrometers, Detect. Assoc. Equip.* 835, 186–225 (2016). <https://doi.org/10.1016/j.nima.2016.06.125>
23. Sihver, L., Sato, T., Gustafsson, K. et al.: Iwase, H., Niita, K., Nakashima, H., Sakamoto, Y., Iwamoto, Y., Matsuda, N.: An update about recent developments of the PHITS code. *Adv. Sp. Res.* 45, 892–899 (2010). <https://doi.org/10.1016/j.asr.2010.01.002>
24. Mashnik, S.G.: Validation and Verification of MCNP6 Against Intermediate and High-Energy Experimental Data and Results by Other Codes. *Eur. Phys. J. Plus.* (2011). <https://doi.org/10.1140/epjp/i2011-11049-1>
25. Goorley, T., James, M., Booth, T. et al.: Features of MCNP6. *Ann. Nucl. Energy.* 87, 772–783 (2016). <https://doi.org/10.1016/J.ANUCENE.2015.02.020>
26. Veenhof, R.: Garfield, recent developments. *Nucl. Instruments Methods Phys. Res. A.* 419, 726–730 (1998). [https://doi.org/10.1016/S0168-9002\(98\)00851-1](https://doi.org/10.1016/S0168-9002(98)00851-1)
27. Smirnov, I.B.: Modeling of ionization produced by fast charged particles in gases. *Nucl. Instruments Methods Phys. Res. Sect. A Accel. Spectrometers, Detect. Assoc. Equip.* 554, 474–493 (2005). <https://doi.org/10.1016/j.nima.2005.08.064>
28. Veenhoff, R., Schindler, H.: Garfield++ – simulation of ionisation based tracking detectors, <http://garfieldpp.web.cern.ch/garfieldpp/>
29. Pfeiffer, D., De Keukeleere, L., Azevedo, C. et al.: A Geant4/Garfield++ and Geant4/Degrad Interface for the Simulation of Gaseous Detectors. (2018)
30. van der Ende, B.M., Rand, E.T., Erlandson, A. et al.: Use of SRIM and Garfield with Geant4 for the characterization of a hybrid 10B/3He neutron detector. *Nucl. Instruments Methods Phys. Res. Sect. A Accel. Spectrometers, Detect. Assoc. Equip.* 894, 138–144 (2018). <https://doi.org/10.1016/J.NIMA.2018.03.056>
31. Lukas, W.: Fast Simulation for ATLAS: Atfast-II and ISF. *J. Phys. Conf. Ser.* 396, 022031 (2012). <https://doi.org/10.1088/1742-6596/396/2/022031>
32. Mokhov, N.V., Gudima, K.K., James, C.C. et al.: Recent enhancements to the MARS15 code. *Radiat Prot Dosim.* 116, 99–103 (2005)
33. Huhtinen, M., Aarnio, P.A.: Neutron and photon fluxes and shielding alternatives for the CMS detector at LHC. *Nucl. Instruments Methods Phys. Res. Sect. A Accel. Spectrometers, Detect. Assoc. Equip.* 363, 545–556 (1995). [https://doi.org/10.1016/0168-9002\(95\)00444-0](https://doi.org/10.1016/0168-9002(95)00444-0)
34. Hrivnacova, I., Adamova, D., Berejnoi, V. et al.: The Virtual Monte Carlo. In: *Computing in High Energy and Nuclear Physics (CHEP03)*, La Jolla, CA. p. arXiv:cs/0306005 (2003)
35. Kalos, M.H., Whitlock, P.A.: *Monte Carlo methods*. Wiley - VCH (2008)
36. James, F.: Monte Carlo theory and practice. *Reports Prog. Phys.* 43, 1145–1189 (1980). <https://doi.org/10.1088/0034-4885/43/9/002>
37. Bielajew, A.F.: *Fundamentals of the Monte Carlo method for neutral and charged particle transport*. (2000)
38. Panneton, F., L'Ecuyer, P.: Resolution-stationary random number generators. *Math. Comput. Simul.* 80, 1096–1103 (2010). <https://doi.org/10.1016/j.matcom.2007.09.014>
39. Savvidy, G., Ter-Arutyunyan-Savvidy, N.: On the Monte Carlo simulation of physical systems. *J. Comput. Phys.* 97, 566–572 (1991). [https://doi.org/10.1016/0021-9991\(91\)90015-D](https://doi.org/10.1016/0021-9991(91)90015-D)
40. Savvidy, K., Savvidy, G.: Spectrum and entropy of C-systems MIXMAX random number generator. *Chaos, Solitons & Fractals.* 91, 33–38 (2016). <https://doi.org/10.1016/j.chaos.2016.05.003>
41. Lüscher, M.: A portable high-quality random number generator for lattice field theory simulations. *Comput. Phys. Commun.* 79, 100–110 (1994). [https://doi.org/10.1016/0010-4655\(94\)90232-1](https://doi.org/10.1016/0010-4655(94)90232-1)
42. James, F.: RANLUX: A Fortran implementation of the high-quality pseudorandom number generator of Lüscher. *Comput. Phys. Commun.* 79, 111–114 (1994). [https://doi.org/10.1016/0010-4655\(94\)90233-X](https://doi.org/10.1016/0010-4655(94)90233-X)

43. L'Ecuyer, P., Simard, R.: TestU01: A C library for empirical testing of random number generators. *ACM Trans. Math. Softw.* 33, 22–es (2007). <https://doi.org/10.1145/1268776.1268777>
44. Berger, M.J.: Monte Carlo calculation of the penetration and diffusion of fast charged particles. In: B. Alder S. Fernbach and Rotenberg, M. (eds.) *Methods in Computational Physics: Advances in Research and Applications*, Vol. 1. Statistical Physics. pp. 135–215. Academic, New York (1963)
45. Ford, R.L., Nelson, W.R.: *The EGS Code System: Computer Programs for the Monte Carlo Simulation of Electromagnetic Cascade Showers (Version 3)*. (1978)
46. Nelson, W.R., Hirayama, H., Rogers, D.W.O.: *The EGS4 code system*. (1985)
47. Salvat, F., Fernández-Varea, J.M.: Overview of physical interaction models for photon and electron transport used in Monte Carlo codes. *Metrologia*. 46, S112–S138 (2009). <https://doi.org/10.1088/0026-1394/46/2/S08>
48. Baró, J., Sempau, J., Salvat, F. et al.: PENELOPE: An algorithm for Monte Carlo simulation of the penetration and energy loss of electrons and positrons in matter. *Nucl. Instruments Methods Phys. Res. B*. 100, 31–46 (1995). [https://doi.org/10.1016/0168-583X\(95\)00349-5](https://doi.org/10.1016/0168-583X(95)00349-5)
49. Goudsmit, S., Saunderson, J.L.: Multiple Scattering of Electrons. II. *Phys. Rev.* 58, 36–42 (1940). <https://doi.org/10.1103/PhysRev.58.36>
50. Molière, G.: Theorie der Streuung schneller geladener Teilchen I. Einzelstreuung am abgeschirmten Coulomb-Feld. *Zeitschrift Naturforsch. Tl. A*. 2, 133–+ (1947)
51. Lewis, H.W.: Multiple Scattering in an Infinite Medium. *Phys. Rev.* 78, 526–529 (1950). <https://doi.org/10.1103/PhysRev.78.526>
52. Bielajew, A.F., Rogers, D.W.O.: Presta: The parameter reduced electron-step transport algorithm for electron monte carlo transport. *Nucl. Instruments Methods Phys. Res. Sect. B Beam Interact. with Mater. Atoms*. 18, 165–171, 174–181 (1986). [https://doi.org/10.1016/S0168-583X\(86\)80027-1](https://doi.org/10.1016/S0168-583X(86)80027-1)
53. Kawrakow, I., Bielajew, A.F.: On the condensed history technique for electron transport. *Nucl. Instruments Methods Phys. Res. B*. 142, 253–280 (1998). [https://doi.org/10.1016/S0168-583X\(98\)00274-2](https://doi.org/10.1016/S0168-583X(98)00274-2)
54. Bielajew, A.F., Salvat, F.: Improved electron transport mechanics in the PENELOPE Monte-Carlo model. *Nucl. Instruments Methods Phys. Res. B*. 173, 332–343 (2001). [https://doi.org/10.1016/S0168-583X\(00\)00363-3](https://doi.org/10.1016/S0168-583X(00)00363-3)
55. Salvat, F., Fernández-Varea, J.M., Sempau, J.: “PENELOPE, A Code System for Monte Carlo Simulation of Electron and Photon Transport.”, Barcelona (2009)
56. Kawrakow, I.: Accurate condensed history Monte Carlo simulation of electron transport. I. EGSnrc, the new EGS4 version. *Med. Phys.* 27, 485–498 (2000)
57. Hirayama, H., Namito, Y., Bielajew, A.F. et al.: The EGS5 code system. (2005)
58. Vilches, M., García-Pareja, S., Guerrero, R. et al.: Monte Carlo simulation of the electron transport through thin slabs: A comparative study of penelope, geant3, geant4, egsrc and mcnp. *Nucl. Instruments Methods Phys. Res. Sect. B Beam Interact. with Mater. Atoms*. 254, 219–230 (2007). <https://doi.org/10.1016/j.nimb.2006.11.061>
59. Incerti, S., Ivanchenko, V., Novak, M.: Recent progress of Geant4 electromagnetic physics for calorimeter simulation. *J. Instrum.* 13, C02054–C02054 (2018). <https://doi.org/10.1088/1748-0221/13/02/C02054>
60. Grichine, V.M., Sadilov, S.S.: Geant4 models for X-ray transition radiation. *Nucl. Instruments Methods Phys. Res. A*. 522, 122–125 (2004). <https://doi.org/10.1016/j.nima.2004.01.031>
61. Armstrong, T.W., Chandler, K.G.: HETC - a high energy transport code. *Nucl. Sci. Eng.* 49, 110–111 (1972)
62. Dementyev, A. V, Sobolevsky, N. M.: SHIELD - Universal Monte Carlo Hadron Transport Code: Scope and Applications. *Radiat. Meas.* 50, 553–557 (1999). [https://doi.org/10.1016/S1350-4487\(99\)00231-0](https://doi.org/10.1016/S1350-4487(99)00231-0)
63. Weisskopf, V.F., Ewing, D.H.: On the Yield of Nuclear Reactions with Heavy Elements. *Phys. Rev.* 57, 472–485 (1940). <https://doi.org/10.1103/PhysRev.57.472>

64. Botvina, A.S., Iljinov, A.S., Mishustin, I.N. et al.: Statistical simulation of the break-up of highly excited nuclei. *Nucl. Phys. A.* 475, 663–686 (1987). [https://doi.org/10.1016/0375-9474\(87\)90232-6](https://doi.org/10.1016/0375-9474(87)90232-6)
65. Furihata, S.: The GEM Code - the Generalized Evaporation Model and the Fission Model. In: A. Kling, Barão, F., Nakagawa, M., Távora, L., and P. Vaz (eds.) *Advanced Monte Carlo for Radiation Physics, Particle Transport Simulation and Applications*. p. 1045–+ (2001)
66. Gudima, K.K., Mashnik, S.G., Toneev, V.D.: Cascade-exciton model of nuclear reactions. *Nucl. Phys. A.* 401, 329–361 (1983). [https://doi.org/10.1016/0375-9474\(83\)90532-8](https://doi.org/10.1016/0375-9474(83)90532-8)
67. Mashnik, S.G., Gudima, K.K., Prael, R.E. et al.: CEM03.03 and LAQGSM03.03 Event Generators for the MCNP6, MCNPX, and MARS15 Transport Codes. (2008). <https://doi.org/10.1016/j.nimb.2010.09.005>
68. Bertini, H.W.: Intranuclear-Cascade Calculation of the Secondary Nucleon Spectra from Nucleon-Nucleus Interactions in the Energy Range 340 to 2900 MeV and Comparisons with Experiment. *Phys. Rev.* 188, 1711–1730 (1969). <https://doi.org/10.1103/PhysRev.188.1711>
69. Bleicher, M., Zabrodin, E., Spieles, C. et al.: Relativistic hadron-hadron collisions in the ultra-relativistic quantum molecular dynamics model. *J. Phys. G Nucl. Part. Phys.* 25, 1859–1896 (1999)
70. Folger, G., Ivanchenko, V.N., Wellisch, J.P.: The Binary Cascade. *Eur. Phys. J. A.* 21, 407–417 (2004). <https://doi.org/10.1140/epja/i2003-10219-7>
71. Heikkinen, A., Stepanov, N., Wellisch, J.P.: Bertini intra-nuclear cascade implementation in Geant4. In: *13th Intern. Computing in High Energy and Nuclear Physics*, (CHEP 2003): La Jolla, California, March 24–28, 2003. p. arXiv:nucl-th/0306008 (2003)
72. Duarte, H.: Particle production in nucleon induced reactions above 14 MeV with an intranuclear cascade model. *Phys. Rev. C.* 75, 24611 (2007). <https://doi.org/10.1103/PhysRevC.75.024611>
73. Degtyarenko, P.V., Kossov, M.V., Wellisch, H.-P.: Chiral invariant phase space event generator. *Eur. Phys. J. A.* 8, 217–222 (2000). <https://doi.org/10.1007/s100500070108>
74. Wright, D.H., Kelsey, M.H.: The Geant4 Bertini Cascade. *Nucl. Instrum. Methods A.* 804, 175–188 (2015). <https://doi.org/10.1016/j.nima.2015.09.058>
75. Boudard, A., Cugnon, J., Leray, S. et al.: Intranuclear cascade model for a comprehensive description of spallation reaction data. *Phys. Rev. C.* 66, 044615 (2002). <https://doi.org/10.1103/PhysRevC.66.044615>
76. Boudard, A., Cugnon, J., David, J.-C. et al.: New potentialities of the Liège intranuclear cascade model for reactions induced by nucleons and light charged particles. *Phys. Rev. C.* 87, 014606 (2013). <https://doi.org/10.1103/PhysRevC.87.014606>
77. Mancusi, D., Boudard, A., Cugnon, J. et al.: Extension of the Liège intranuclear-cascade model to reactions induced by light nuclei. *Phys. Rev. C.* 90, 054602 (2014). <https://doi.org/10.1103/PhysRevC.90.054602>
78. Napolitani, P., Schmidt, K.-H., Botvina, A.S. et al.: High-resolution velocity measurements on fully identified light nuclides produced in Fe 56 + hydrogen and Fe 56 + titanium systems. *Phys. Rev. C.* 70, 054607 (2004). <https://doi.org/10.1103/PhysRevC.70.054607>
79. Ricciardi, M. V., Armbruster, P., Benlliure, J. et al.: Light nuclides produced in the proton-induced spallation of U 238 at 1 GeV. *Phys. Rev. C.* 73, 014607 (2006). <https://doi.org/10.1103/PhysRevC.73.014607>
80. Leray, S., David, J.C., Khandaker, M. et al.: Results from the IAEA Benchmark of Spallation Models. *J. Korean Phys. Soc.* 59, 791 (2011). <https://doi.org/10.3938/jkps.59.791>
81. Akchurin, N., Bedeschi, F., Cardini, A. et al.: Lessons from Monte Carlo simulations of the performance of a dual-readout fiber calorimeter. *Nucl. Instruments Methods Phys. Res. Sect. A Accel. Spectrometers, Detect. Assoc. Equip.* 762, 100–118 (2014). <https://doi.org/10.1016/J.NIMA.2014.05.121>
82. Capella, A., Sukhatme, U., Tan, C.-I. et al.: Dual parton model. *Phys. Rep.* 236, 225–329 (1994). [https://doi.org/10.1016/0370-1573\(94\)90064-7](https://doi.org/10.1016/0370-1573(94)90064-7)

83. Kaidalov, A.B.: Interactions of hadrons and nuclei at superhigh energies and small-x physics. Nucl. Phys. B Proc. Suppl. 75, 81–88 (1999). [https://doi.org/10.1016/S0920-5632\(99\)00218-2](https://doi.org/10.1016/S0920-5632(99)00218-2)
84. Ostapchenko, S.: QGSJET-II: towards reliable description of very high energy hadronic interactions. Nucl. Phys. B Proc. Suppl. 151, 143–146 (2006). <https://doi.org/10.1016/j.nuclphysbps.2005.07.026>
85. Uzhinsky, V., Apostolakis, J., Galoyan, A. et al.: Antinucleus and nucleus cross sections implemented in Geant4. Phys. Lett. B. 705, 235–239 (2011). <https://doi.org/10.1016/j.physletb.2011.10.010>
86. Uzhinsky, V., Galoyan, A.: Effect of $u\bar{u}$ diquark suppression in proton splitting in Monte Carlo event generators. Phys. Rev. D. 91, 037501 (2015). <https://doi.org/10.1103/PhysRevD.91.037501>
87. Koning, A.J. et al.: The JEFF evaluated nuclear data project. In: O. Bersillon F. Gunsing, E.B.R.J. and S. Leray (eds.) International Conference on Nuclear Data for Science and Technology 2007 (April 22–27, 2007, Nice, France). pp. 194–199. EDP Sciences (2008)
88. Chadwick, M.B., Obložinský, P., Herman, M. et al.: ENDF/B-VII.0: Next Generation Evaluated Nuclear Data Library for Nuclear Science and Technology. Nucl. Data Sheets. 107, 2931–3060 (2006). <https://doi.org/10.1016/j.nds.2006.11.001>
89. Brown, D.A., Chadwick, M.B., Capote, R. et al.: ENDF/B-VIII.0: The 8th Major Release of the Nuclear Reaction Data Library with CIELO-project Cross Sections, New Standards and Thermal Scattering Data. Nucl. Data Sheets. 148, 1–142 (2018). <https://doi.org/10.1016/j.nds.2018.02.001>
90. Shibata, K., Iwamoto, O., Nakagawa, T. et al.: JENDL-4.0: A New Library for Nuclear Science and Engineering. J. Nucl. Sci. Technol. 48, 1–30 (2011). <https://doi.org/10.1080/18811248.2011.9711675>
91. Ge, Z.G., Zhao, Z.X., Xia, H.H. et al.: The Updated Version of Chinese Evaluated Nuclear Data Library (CENDL-3.1). J. Korean Phys. Soc. 59, 1052–1056 (2011). <https://doi.org/10.3938/jkps.59.1052>
92. Kossov, M.V.: Chiral-invariant phase space model. Eur. Phys. J. A - Hadron. Nucl. 14, 265–269 (2002). <https://doi.org/10.1140/epja/i2001-10211-3>
93. Gabriel, T.A., Groom, D.E., Job, P.K. et al.: Energy dependence of hadronic activity. Nucl. Instruments Methods Phys. Res. Sect. A Accel. Spectrometers, Detect. Assoc. Equip. 338, 336–347 (1994). [https://doi.org/10.1016/0168-9002\(94\)91317-X](https://doi.org/10.1016/0168-9002(94)91317-X)
94. Wigmans, R.: Calorimetry : Energy measurement in particle physics. Clarendon Press (2000)
95. Groom, D.E.: Energy flow in a hadronic cascade: Application to hadron calorimetry. Nucl. Instruments Methods Phys. Res. Sect. A Accel. Spectrometers, Detect. Assoc. Equip. 572, 633–653 (2007). <https://doi.org/10.1016/j.nima.2006.11.070>
96. de Favereau, J., Delaere, C., Demin, P. et al.: DELPHES 3: a modular framework for fast simulation of a generic collider experiment. J. High Energy Phys. 57 (2014). [https://doi.org/10.1007/JHEP02\(2014\)057](https://doi.org/10.1007/JHEP02(2014)057)
97. Giammanco, A.: The Fast Simulation of the CMS Experiment. J. Phys. Conf. Ser. 513, 022012 (2014). <https://doi.org/10.1088/1742-6596/53/2/022012>
98. Ritsch, E., Collaboration, the A.: Concepts and Plans towards fast large scale Monte Carlo production for the ATLAS Experiment. J. Phys. Conf. Ser. 523, 012035 (2014). <https://doi.org/10.1088/1742-6596/523/1/012035>
99. Paganini, M., de Oliveira, L., Nachman, B.: CaloGAN: Simulating 3D high energy particle showers in multilayer electromagnetic calorimeters with generative adversarial networks. Phys. Rev. D. 97, 014021 (2018). <https://doi.org/10.1103/PhysRevD.97.014021>
100. Wigmans, R.: Toward Meaningful Simulations of Hadronic Showers. In: M. Albrow & R. Raja (ed.) Hadronic Shower Simulation Workshop. pp. 123–136 (2007)
101. Smirnov, I.B.: Modeling of ionization produced by fast charged particles in gases. Nucl. Instruments Methods Phys. Res. Sect. A Accel. Spectrometers, Detect. Assoc. Equip. 554, 474–493 (2005). <https://doi.org/10.1016/j.nima.2005.08.064>

102. Biagi, S.F.: Monte Carlo simulation of electron drift and diffusion in counting gases under the influence of electric and magnetic fields. *Nucl. Instruments Methods Phys. Res. Sect. A Accel. Spectrometers, Detect. Assoc. Equip.* 421, 234–240 (1999). [https://doi.org/10.1016/S0168-9002\(98\)01233-9](https://doi.org/10.1016/S0168-9002(98)01233-9)
103. Fedoseyev, A.I., Turowski, M., Alles, M.L. et al.: Accurate numerical models for simulation of radiation events in nano-scale semiconductor devices. *Math. Comput. Simul.* 79, 1086–1095 (2008). <https://doi.org/10.1016/j.matcom.2007.09.013>
104. Schrimpf, R.D., Weller, R.A., Mendenhall, M.H. et al.: Physical mechanisms of single-event effects in advanced microelectronics. *Nucl. Instruments Methods Phys. Res. Sect. B Beam Interact. with Mater. Atoms.* 261, 1133–1136 (2007). <https://doi.org/10.1016/j.nimb.2007.04.050>
105. Bielajew, A.F., Rogers, D.W.O.: Variance-reduction techniques. In: Jenkins, T.E., Nelson, W.R., Rindi, A., Nalum, A.E., and Rogers, D.W.O. (eds.) *Monte Carlo Transport of Electrons and Photons*. pp. 407–420. Plenum Press, New York (1990)
106. Abe, F., Akimoto, H., Akopian, A. et al.: Observation of Top Quark Production in $p\bar{p}$ Collisions with the Collider Detector at Fermilab. *Phys. Rev. Lett.* 74, 2626–2631 (1995). <https://doi.org/10.1103/PhysRevLett.74.2626>
107. Abachi, S., Abbott, B., Abolins, M. et al.: Observation of the Top Quark. *Phys. Rev. Lett.* 74, 2632–2637 (1995). <https://doi.org/10.1103/PhysRevLett.74.2632>
108. Abachi, S., Abolins, M., Acharya, B.S. et al.: The D{Ø} detector. *Nucl. Instruments Methods Phys. Res. Sect. A Accel. Spectrometers, Detect. Assoc. Equip.* 338, 185–253 (1994). [https://doi.org/10.1016/0168-9002\(94\)91312-9](https://doi.org/10.1016/0168-9002(94)91312-9)
109. Collaboration, D., Abazov, V.M., Abbott, B. et al.: Evidence for production of single top quarks. *Phys. Rev. D.* 78, 12005 (2008). <https://doi.org/10.1103/PhysRevD.78.012005>
110. Poon, E., Verhaegen, F.: Accuracy of the photon and electron physics in GEANT4 for radiotherapy applications. *Med. Phys.* 32, 1696–1711 (2005). <https://doi.org/10.1118/1.1895796>
111. Aharrouché, M., Colas, J., Ciaccio, L. et al.: Energy linearity and resolution of the ATLAS electromagnetic barrel calorimeter in an electron test-beam. *Nucl. Instruments Methods Phys. Res. Sect. A Accel. Spectrometers, Detect. Assoc. Equip.* 568, 601–623 (2006). <https://doi.org/10.1016/j.nima.2006.07.053>
112. Khamov, E., Rusakovich, N., Carli, T. et al.: Study of the Response of the Hadronic Barrel Calorimeter in the ATLAS Combined Test-beam to Pions of Energies from 20 to 350 GeV for Beam Impact Points from 0.2 to 0.65. Geneva (2009)
113. Adragna, P., Alexa, C., Anderson, K. et al.: Measurement of pion and proton response and longitudinal shower profiles up to 20 nuclear interaction lengths with the ATLAS Tile calorimeter. *Nucl. Instruments Methods Phys. Res. Sect. A Accel. Spectrometers, Detect. Assoc. Equip.* 615, 158–181 (2010). <https://doi.org/10.1016/j.nima.2010.01.037>
114. Drozhdin, A.I., Huhtinen, M., Mokhov, N.V.: Accelerator related background in the CMS detector at LHC. *Nucl. Instruments Methods Phys. Res. Sect. A Accel. Spectrometers, Detect. Assoc. Equip.* 381, 531–544 (1996). [https://doi.org/10.1016/S0168-9002\(96\)00807-8](https://doi.org/10.1016/S0168-9002(96)00807-8)
115. Aaboud, M., Aad, G., Abbott, B. et al.: A measurement of the calorimeter response to single hadrons and determination of the jet energy scale uncertainty using LHC Run-1 pp-collision data with the ATLAS detector. *Eur. Phys. J. C.* 77, 26 (2017). <https://doi.org/10.1140/epjc/s10052-016-4580-0>
116. CMS: Determination of jet energy calibration and transverse momentum resolution in CMS. *J. Instrum.* 6, P11002–P11002 (2011). <https://doi.org/10.1088/1748-0221/6/11/P11002>
117. Rahmat, R., Kroeger, R., Giammanco, A.: The Fast Simulation of The CMS Experiment. *J. Phys. Conf. Ser.* 396, 062016 (2012). <https://doi.org/10.1088/1742-6596/396/6/062016>
118. Grindhammer, G., Rudowicz, M., Peters, S.: The fast simulation of electromagnetic and hadronic showers. *Nucl. Instruments Methods Phys. Res. Sect. A Accel. Spectrometers, Detect. Assoc. Equip.* 290, 469–488 (1990). [https://doi.org/10.1016/0168-9002\(90\)90566-O](https://doi.org/10.1016/0168-9002(90)90566-O)
119. Sekmen, S., Collaboration, for the C.: Recent Developments in CMS Fast Simulation. (2017)

120. Adloff, C., Blaha, J., Blaising, J.-J. et al.: Validation of GEANT4 Monte Carlo models with a highly granular scintillator-steel hadron calorimeter. *J. Instrum.* 8, P07005 (2013). <https://doi.org/10.1088/1748-0221/8/07/P07005>
121. Santana, G., Nieminen, P., Evansa, H. et al.: New Geant4 based simulation tools for space radiation shielding and effects analysis. *Nucl. Phys. B - Proc. Suppl.* 125, 69–74 (2003). [https://doi.org/10.1016/S0920-5632\(03\)90968-6](https://doi.org/10.1016/S0920-5632(03)90968-6)
122. Santin, G., Ivanchenko, V., Evans, H. et al.: GRAS: a general-purpose 3-D Modular Simulation tool for space environment effects analysis. *IEEE Trans. Nucl. Sci.* 52, 2294–2299 (2005). <https://doi.org/10.1109/TNS.2005.860749>
123. Gillam, J.E., Rafecas, M.: Monte-Carlo simulations and image reconstruction for novel imaging scenarios in emission tomography. *Nucl. Instruments Methods Phys. Res. Sect. A Accel. Spectrometers, Detect. Assoc. Equip.* 809, 76–88 (2016). <https://doi.org/10.1016/J.NIMA.2015.09.084>
124. Castiglioni, I., Cremonesi, O., Gilardi, M.C. et al.: Scatter correction techniques in 3D PET: a Monte Carlo evaluation. *IEEE Trans. Nucl. Sci.* 46, 2053–2058 (1999). <https://doi.org/10.1109/23.819282>
125. Strulab, D., Santin, G., Lazaro, D. et al.: GATE (geant4 application for tomographic emission): a PET/SPECT general-purpose simulation platform. *Nucl. Phys. B - Proc. Suppl.* 125, 75–79 (2003). [https://doi.org/10.1016/S0920-5632\(03\)90969-8](https://doi.org/10.1016/S0920-5632(03)90969-8)
126. Arce, P., Lagares, J.I., Harkness, L. et al.: GAMOS: An easy and flexible way to use GEANT4. In: 2011 IEEE Nuclear Science Symposium Conference Record. pp. 2230–2237. IEEE (2011)
127. España, S., Herraiz, J.L., Vicente, E. et al.: PeneloPET, a Monte Carlo PET simulation tool based on PENELOPE: features and validation. *Phys. Med. Biol.* 54, 1723–1742 (2009). <https://doi.org/10.1088/0031-9155/54/6/021>
128. Barret, O., Carpenter, T.A., Clark, J.C. et al.: Monte Carlo simulation and scatter correction of the GE Advance PET scanner with SimSET and Geant4. *Phys. Med. Biol.* 50, 4823–4840 (2005). <https://doi.org/10.1088/0031-9155/50/20/006>
129. Kawrakow, I., Mitev, K., Gerganov, G. et al.: SU-GG-I-109: Using EGSnrc Within GATE to Improve the Efficiency Of positron Emission Tomography Simulations. *Med. Phys.* 35, 2667–2667 (2008). <https://doi.org/10.1118/1.2961507>
130. Seco, J.: Monte carlo techniques in radiation therapy. CRC Press (2016)
131. Zacharatos Jarlskog, C., Paganetti, H.: Physics Settings for Using the Geant4 Toolkit in Proton Therapy. *IEEE Trans. Nucl. Sci.* 55, 1018–1025 (2008). <https://doi.org/10.1109/TNS.2008.922816>
132. Paganetti, H., Jiang, H., Parodi, K. et al.: Clinical implementation of full Monte Carlo dose calculation in proton beam therapy. *Phys. Med. Biol.* 53, 4825–4853 (2008). <https://doi.org/10.1088/0031-9155/53/17/023>
133. Paganetti, H., Jiang, H., Adams, J.A. et al.: Monte Carlo simulations with time-dependent geometries to investigate effects of organ motion with high temporal resolution. *Int. J. Radiat. Oncol. Biol. Phys.* 60, 942–50 (2004). <https://doi.org/10.1016/j.ijrobp.2004.06.024>
134. Aso, T., Yamashita, T., Akagi, T. et al.: Validation of PTSIM for clinical usage. In: IEEE Nuclear Science Symposium & Medical Imaging Conference. pp. 158–160. IEEE (2010)
135. Perl, J., Shin, J., Schümann, J. et al.: TOPAS: An innovative proton Monte Carlo platform for research and clinical applications. *Med. Phys.* 39, 6818–6837 (2012). <https://doi.org/10.1118/1.4758060>
136. Böhlen, T.T., Cerutti, F., Dosanjh, M. et al.: Benchmarking nuclear models of FLUKA and GEANT4 for carbon ion therapy. *Phys. Med. Biol.* 55, 5833–5847 (2010). <https://doi.org/10.1088/0031-9155/55/19/014>
137. Dedes, G., Pinto, M., Dauvergne, D. et al.: Assessment and improvements of Geant4 hadronic models in the context of prompt-gamma hadrontherapy monitoring. *Phys. Med. Biol.* 59, 1747–1772 (2014). <https://doi.org/10.1088/0031-9155/59/7/1747>

138. Mairani, A., Brons, S., Cerutti, F. et al.: The FLUKA Monte Carlo code coupled with the local effect model for biological calculations in carbon ion therapy. *Phys. Med. Biol.* 55, 4273–4289 (2010). <https://doi.org/10.1088/0031-9155/55/15/006>
139. Robert, C., Dedes, G., Battistoni, G. et al.: Distributions of secondary particles in proton and carbon-ion therapy: a comparison between GATE/Geant4 and FLUKA Monte Carlo codes. *Phys. Med. Biol.* 58, 2879–99 (2013). <https://doi.org/10.1088/0031-9155/58/9/2879>
140. De Napoli, M., Agodi, C., Battistoni, G. et al.: Carbon fragmentation measurements and validation of the Geant4 nuclear reaction models for hadrontherapy. *Phys. Med. Biol.* 57, 7651–7671 (2012). <https://doi.org/10.1088/0031-9155/57/22/7651>
141. Battistoni, G., Bauer, J., Boehlen, T.T. et al.: The FLUKA Code: An Accurate Simulation Tool for Particle Therapy. *Front. Oncol.* 6, 116 (2016). <https://doi.org/10.3389/fonc.2016.00116>
142. Nikjoo, H., Uehara, S., Emfietzoglou, D. et al.: Track-structure codes in radiation research. *Radiat. Meas.* 41, 1052–1074 (2006). <https://doi.org/10.1016/j.radmeas.2006.02.001>
143. El Naqa, I., Pater, P., Seuntjens, J.: Monte Carlo role in radiobiological modelling of radiotherapy outcomes, (2012)
144. Bernal, M.A., Bordage, M.C., Brown, J.M.C. et al.: Track structure modeling in liquid water: A review of the Geant4-DNA very low energy extension of the Geant4 Monte Carlo simulation toolkit. *Phys. Medica.* 31, 861–874 (2015). <https://doi.org/10.1016/J.EJMP.2015.10.087>
145. Incerti, S., Douglass, M., Penfold, S. et al.: Review of Geant4-DNA applications for micro and nanoscale simulations. *Phys. Medica.* 32, 1187–1200 (2016). <https://doi.org/10.1016/J.EJMP.2016.09.007>
146. Pedoux, S., Cugnon, J.: Extension of the Liège intranuclear cascade model at incident energies between 2 and 12 GeV. Aspects of pion production. *Nucl. Phys. A.* 866, 16–36 (2011)
147. Dingfelder, M., Ritchie, R.H., Turner, J.E. et al.: Comparisons of calculations with PARTRAC and NOREC: transport of electrons in liquid water. *Radiat. Res.* 169, 584–594 (2008). <https://doi.org/10.1667/RR1099.1>
148. Thomson, M.A.: Particle flow calorimetry and the PandoraPFA algorithm. *Nucl. Instruments Methods Phys. Res. Sect. A Accel. Spectrometers, Detect. Assoc. Equip.* 611, 25–40 (2009). <https://doi.org/10.1016/j.nima.2009.09.009>
149. Aduszkiewicz, A., Ali, Y., Andronov, E. et al.: Measurements of π^\pm , K^\pm , p and p-bar spectra in proton-proton interactions at 20, 31, 40, 80 and 158 GeV/c with the NA61/SHINE spectrometer at the CERN SPS. *Eur. Phys. J. C.* 77, 671 (2017). <https://doi.org/10.1140/epjc/s10052-017-5260-4>

Open Access This chapter is licensed under the terms of the Creative Commons Attribution 4.0 International License (<http://creativecommons.org/licenses/by/4.0/>), which permits use, sharing, adaptation, distribution and reproduction in any medium or format, as long as you give appropriate credit to the original author(s) and the source, provide a link to the Creative Commons licence and indicate if changes were made.

The images or other third party material in this chapter are included in the chapter's Creative Commons licence, unless indicated otherwise in a credit line to the material. If material is not included in the chapter's Creative Commons licence and your intended use is not permitted by statutory regulation or exceeds the permitted use, you will need to obtain permission directly from the copyright holder.

